SYNCHRONIZATION IN IMPULSE BASED ULTRA WIDEBAND SYSTEMS.

Dinakara Phaneendra Kumar Piratla

Thesis submitted to the Faculty of the Virginia Polytechnic Institute and State University in partial fulfillment of the requirement for the degree of

Master of Science
In
Electrical Engineering

Dr. Amir I. Zaghloul, Chair
Dr. Saifur Rahman
Dr. Jeffrey H. Reed

June 9th 2008

Keywords: Direct Sequence UWB, Impulse Radio, Synchronization, Time Hopping UWB, Ultra Wideband, UWB

Synchronization in Impulse Based Ultra Wideband Systems

Dinakara Phaneendra Kumar Piratla

ABSTRACT

In Impulse Radio based Ultra Wide Band (UWB) systems, where sub-nano second pulses are used, synchronization is very challenging because of their short pulse duration and very low duty cycle.

Coherent detection of ultra wide-band signals requires complex channel estimation algorithms. In impulse based UWB systems, suboptimal receivers that require no channel estimation are proposed for low data rate applications using non coherent detection of energy. This approach requires integrators that collect energy and detect the incoming stream of bits for detection and synchronization. These techniques yield reasonable performance when compared to coherent detection techniques that require complex hardware and dissipate more energy.

Non-coherent detection is a promising technique for low complexity, low cost and low data rate ultra-wideband communication applications like sensor area networks. In the past, several attempts have been made to characterize the performance of the energy collection receivers for synchronization using various metrics that include time of arrival and BER measurements. A comprehensive study of the synchronization problem using Probability of False Alarm is limited. The current thesis attempts to characterize the synchronization problem using Probability of False Alarm and Probability of Detection under various channel models and also discusses the importance of the length of the integration window for energy collection receivers.

The current work also focuses on the performance evaluation of synchronization for Impulse based UWB systems using energy capture method and modeling them using the Probability of False Alarm and Probability of Detection under various channel models. In these systems, the integration region of a receiver integrator significantly affects the bit error rate (BER) performance. The effect of the integration window on the performance of the algorithm is also studied.

This work also discusses the trade-offs between complexity and precision in using these algorithms for synchronization of Impulse based Direct Sequence Ultra Wideband Systems (DS-UWB). Signal to Noise Ratio vs. Probability of Detection, Probability of False Alarm are plotted for different channel models.

ACKNOWLEDGEMENTS

It was an honor to work with a great group of professors and students at Virginia Tech. I am greatly indebted to my advisor Dr. Amir Zaghloul for his ideas and support through out my M.S. studies. He was always accessible and highly motivating.

I am very thankful to Dr. Saifur Rahman providing financial support through out my M.S. studies. He always reminded me that school duties should be my first priority. His support through my graduate studies was very instrumental for my success at Virginia Tech. I express my gratitude to Dr. Jeffrey Reed for all the support he had extended to me in the past few years. His research ideas were always much thought provoking and intellectually stimulating. I am also indebted to him for his valuable comments and suggestions on my work that helped me write a better thesis.

My stay at Virginia Tech would not have been so much fun without my friends Dr. Praveed Edara, Sai Krovvidi, Vishal Kothari, Prajwal Manalwar, and many more. Thank you all for the memorable times.

Finally, I am grateful to my wife and parents for their unconditional love, encouragement and sacrifices they have done for my education; and to my brother and sister-in-law for their love, understanding, and support.

TABLE OF CONTENTS

List of Figures

Chapter 1

Introduction

1.1 UWB and Personal Area Networks

Ultra-wideband usually refers to a radio communications technique based on transmitting very-short-duration pulses, often of duration of only nanoseconds or less, whereby the occupied bandwidth goes to very large values. The introduction of UWB never goes without mentioning an important date in its history in February 2002; FCC allocated a spectrum from 3.1 to 10.6 GHz for unlicensed indoor use of UWB devices. FCC also defined Ultra Wideband as a signal having a 10dB bandwidth greater than 500 MHz [1].

The history of impulse radio dates back to the seventies when it was used for Radar applications. UWB has been used primarily for the Ground Penetrating Radar (GPR) projects until recently when people discovered the promise of UWB in the area of personal area networks.

As always, every technology finds its applications according to the properties it possesses. UWB has the following properties after applying the FCC rules:

1. Low Power.
2. Short range.
3. High Bandwidth.

The low power nature of UWB can be utilized in the area of sensor networks and military applications where the battery power plays an important role in the life of a node in a sensor network. FCC's imposed power mask of -41.3dBm/MHz combined with huge bandwidth makes UWB a promising technology in the area of Wireless Personal Area Networks.

According to Shannon's theorem, high bandwidth comes with higher data rates. This higher bandwidth together with short range provides a great alternative for cable replacement inside homes and for streaming high quality video applications wirelessly to a HD tuned receiver. Other typical applications include transfer of videos, pictures and multimedia content from phones/PDA's to UWB enabled devices. UWB enabled high resolution PC monitors are not far from reality.

The market for UWB over USB for a wireless USB is definitely promising. Research by In-Stat [2] found that over 289 Million UWB Chipsets will be shipped by 2010 making UWB one of the core technologies to be used by human beings.

1.2 Multiband OFDM and Direct Sequence UWB Approach

Ultra Wideband (UWB) is defined as any signal having a 10dB bandwidth of greater than 500 MHz. The IEEE 803.15.3 working group has come up with two approaches for standardizing Ultra Wideband before the group fell apart with no consensus for the standard. The proposals from WiMedia alliance [3] with OFDM based PHY and the

UWB Forum [4] with Direct Sequence UWB were considered as strong candidates for the 802.15.3a standard before the dissolution of the group to form a standard.

1.2.1 Multiband OFDM Approach

Multiband OFDM approach for UWB is based on multiple OFDM bands each with at least 500 MHz bandwidth and each OFDM band comprising multiple sub-carriers. It can also be thought of as a combination of Frequency Hopping (FH) with the sub-carriers occupying one band at one time and hopping according to a pre-defined hopping pattern.

This method takes advantages of all the features inherent in the OFDM, like reducing the Inter Symbol Interference (ISI) due to multipath and thus eliminating the need for a complex equalizer in the RF chain. It also takes advantages of Frequency Hopping by effectively mitigating mutual interference between the piconets and achieving frequency diversity across sub-bands of an UWB network.

The system also comes with the disadvantages inherent in OFDM like the tight channel spacing increases the receiver's sensitivity to frequency synchronization resulting in poor performance also leading to high peak-to-average power ratio requiring highly linear electronics to handle highly variable power requirements [5].

1.2.2 Direct Sequence (DS-UWB) Approach

As the name indicates, the DS-UWB is based on the Direct Sequence Spread Spectrum used in the conventional CDMA cellular networks. The main attractive part of this approach is simplicity as these techniques do not require any analog up or down

conversion and avoiding all interference rejection filtering. A data stream is applied to pulses using bi-orthogonal keying or pulse position modulation which results in a carrier-less signal that occupies the spectrum allocated by the FCC from 3.1 to 10.6 GHz.

Accordingly, each data symbol is spread by an orthogonal code to form the transmit chip sequence. Rake receivers are employed to collect the signal energy of the multipath components achieving much higher processing gain. The advantages of this include the mitigation of mutual interference between piconets. While the simplicity of this kind of Impulse Based UWB might seem straight forward, difficulties arise in realizing the RF circuitry, like wide band non-dispersive amplifiers and antennas. Another challenge of using DS UWB is that Inter Symbol Interference that can severely degrade the performance of the entire system and necessitates the use of equalizer at the receiver. Also, there are major challenges for the DSP engines used to recover the data over a highly corrupted channel.

There are various forms of pulses that can be used to represent these impulses in a Direct Sequence UWB system. Gaussian Monocycle Wavelets and their derivatives in the time domain are the chosen waveforms for Impulse Radio applications [8]. Gaussian duo pulse is chosen for the current work which is outside the limits of the FCC mask. As the receiver is based on signal energy collection, the same results can be obtained from an FCC compliant waveform.

1.3 Motivation

The complexity of a receiver for synchronization with the transmitter is very high for a system that uses sub-nano second pulses like UWB because of the high bandwidth associated with these pulses. The synchronization is one of the very important aspects for sub nano second and low duty cycle pulses of Impulse Radio UWB. When the pulses are transmitted within the FCC limits, the receiver has to dig the pulse information sometimes below the noise floor. The process of synchronization is also helpful in the channel estimation of Impulse Radio based UWB systems.

The challenges involved in designing and synchronizing the sub nano second pulses is a daunting task unlike the conventional narrow band systems. This work discusses the important aspect of the initial coarse synchronization of DS-UWB based systems at the receiver and proposes a simplified solution for achieving the synchronization of low duty cycle pulses using energy capture techniques. The precision of the algorithm can be enhanced by increasing the complexity (in the number of parallel integrators) of the algorithm.

1.4 Organization of the Thesis

Following this introduction, Chapter 2 introduces Impulse Radio transmitter and receiver architectures followed by the promise of UWB, multipath interference and regulatory issues. The ideal noiseless case is explained followed by the effects of noise in these receivers and the application of the energy collection in the synchronization of UWB

pulses is studied. Chapter 3 explains the modified Saleh Valenzuela channel models studied as part of this work. Chapter 4 describes the details of the synchronization scheme used in this work along with the flow chart of the algorithm. The Probability of Detection and the Probability of False Alarm are introduced in this chapter. Various simulation results are detailed for the modified S-V channel models. Chapter 4 concludes by discussing the effect of the integration window on the performance of the algorithm for all four channel conditions of modified Saleh Valenzuela model. The final chapter deals with the conclusions and future research work that can be carried on the current subject.

1.5 Extension of Previous Work

The synchronization algorithm dealt in this thesis is based on the work from [6] which uses energy collection approach for synchronization. The current thesis chooses *Probability of False Alarm* as the criteria for the evaluation of the energy collection approach. The current work also evaluates the importance of the integration window in energy collection receivers under various channel conditions proposed for wireless personal area networks. Also, the current thesis is simulated under the modified Saleh Valenzuela models proposed by the IEEE 803.15.3 study group.

Simulations are performed for various channel conditions of S-V models and the results are plotted using the Signal to Noise Ratio (SNR) vs. Probability of False Alarm graphs.

Chapter 2

Synchronization in Impulse Based UWB Systems

This chapter provides an insight into the concepts of Impulse Radio including the block diagram of a UWB system and discusses the concept of energy collection receivers. The important concept of synchronization using energy collection receivers is detailed and the effect of noise on the synchronization of these energy collection receivers is considered.

2.1 Impulse Radio Overview

Impulse Radio is a type of communication where sub nano second pulses are used in spreading the signal to a few Giga Hertz range. Further spreading of these pulses is achieved by time hopping these low duty cycle pulses and the data modulation is accomplished by additional pulse position modulation. The UWB waveform used in this paper is the 2" derivative of the Gaussian pulse which lies outside the limits of the FCC mask. As the receiver is based on signal energy collection, the same results can be obtained with an FCC compliant pulse waveform [6]. The width of the pulse determines the center frequency of the UWB signal. For example, if the pulse width is 320ps, the pulse would have a center frequency of 3.125GHz (1/320ps). For a shorter pulse such as 95ps, the center frequency is 10.6GHz. Low power transmission is a key characteristic

that allows UWB technology to coexist with other wireless technologies. As Impulse Radio based UWB doesn't use any carrier signal, it is also called as baseband or carrierless or zero-carrier technology. Hence, impulse based UWB can drive its antenna directly with a baseband signal.

2.1.1 Transmitter Architecture

The transmitted signal of a PPM based UWB signal from [6] is represented as shown in the equation (1) below:

$$s(t) = \sum_{k=-\infty}^{\infty} w_{tr}(t - kT_b - jT_c - T_s d_k)(c_p)_j \qquad (1)$$

Where $w_{tr}(t)$ is the transmitted pulse waveform with pulse width T_p.

T_b is the symbol interval.

T_s is the time shift used to distinguish different symbols and

d_k is the k^{th} transmitted symbol given by $d_k \in [0,1,....M-1]$

$T_c = NT_p$ where N is the chip interval.

$(c_p)_j$ is the j^{th} chip of the pseudo-random (PR) code which is either a -1 or a 1.

$R_d = 1/T_b$ is the data rate.

The transceiver portion of a PPM based UWB system can be implemented in digital CMOS and doesn't require expensive SAW filters common to conventional radio technologies. The functional block diagram of a UWB transmitter is shown in Figure 2.1 below. The pulse forming network creates the impulses monitored by a PLL, modulated by the input data bits and is directly fed to the antenna. There are no amplifiers involved as these pulses can drive the antenna. The advantage of this system is its simplicity in construction without having any amplifiers or expensive electronics.

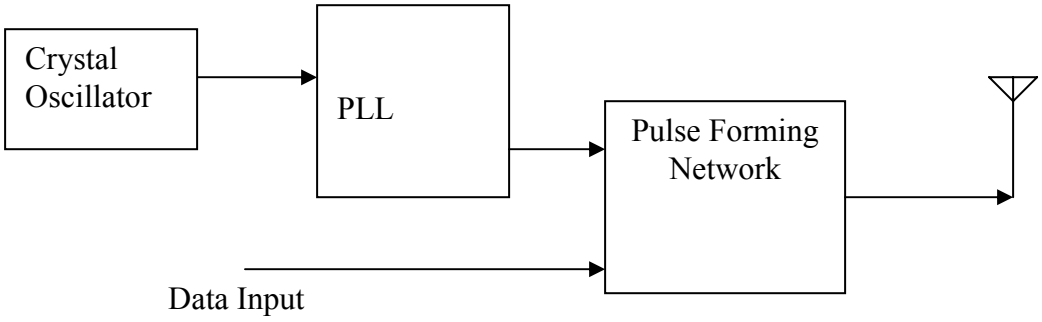

Figure 2.1: Functional Block Diagram of a UWB Transmitter

2.1.2 Receiver Architecture

The received signal for the UWB waveform described above is given by Eq (2):

$$s_r(t) = \sum_{l=0}^{L} A_i \sum_{k=-\infty}^{\infty} \sum_{j=1}^{N} w_{rx}(t - kT_b - jT_c - T_s d_k - \tau_l)(c_p)_j + n(t) \qquad (2)$$

Where $w_{rx}(t)$ is the received signal and the first derivative of $w_{tx}(t)$ as the UWB antenna acts as a differentiator [7] to produce naturally at its output the first derivative of the input pulse.

L is the number of resolvable paths,

A_i is the gain for path i and $n(t)$ is the zero mean additive Gaussian noise.

The UWB waveform $w_{tx}(t)$ used here is the first derivative of Gaussian pulse and $w_{rx}(t)$ is the second derivative of Gaussian pulse.

The functional block diagram of a UWB receiver is shown in Figure 2.2 below.

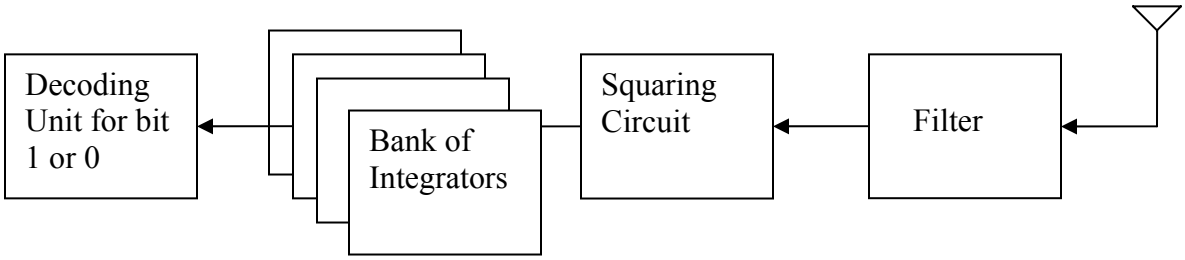

Figure 2.2: Functional Block Diagram of a UWB Receiver

The typical UWB receiver consists of a filter followed by the squaring circuit that is fed into a bank of integrators (Energy Collection) separated in time followed by the decoding unit for the integrator that corresponds to the maximum energy.

2.1.3 Channel Capacity and the Promise of UWB

According to Shannon's theorem, the maximum Channel capacity C (bits/sec) of a communication system is given by:

$$C = B\ log_2 \left(1 + \frac{S}{N}\right) \qquad (3)$$

Because of the constraints imposed by the regulatory bodies, UWB devices operate at very low SNR values.

Hence when $\left(\frac{S}{N}\right) << 0$, then $log_2 \quad \left(1 + \frac{S}{N}\right) \cong \frac{S}{N}$

Replacing the above equation in equation (3), we have the channel capacity as:

$$C = B\ log_2 \left(1 + \frac{S}{N}\right) \cong B\frac{S}{N} \qquad (4)$$

Hence, the channel capacity is proportional to the bandwidth for low SNR signals. The potential of UWB can be used to increase the channel capacity because of its inherent properties of low SNR and high bandwidth (> 500MHz) and data rates of more than 500Mbps can be achieved using such systems. For a communication system with significant signal to noise ratio, equation (3) can be written as below:

$$C \cong B\ log_2 \left(\frac{S}{N}\right) \qquad (5)$$

For example, in a typical 802.11a system with a 54Mbps data rate having a bandwidth of 20MHz, the SNR values are around 26dB. For obtaining higher data rates, the complexity of the system has to be increased significantly.

2.1.4 Multipath Interference

Each pulse in a UWB system can occupy the entire spectrum allocated for UWB by the FCC, thus reaping the benefits of relative immunity to multipath fading, unlike the narrow band systems that are subject to both deep fades and intersymbol interference. Multipath resolution down to a nanosecond in differential path delay (equivalently down to a differential path length of 1 ft) leads to an elimination of significant multipath fading. This may considerably reduce fading margins in link budgets and may allow low transmission power operations. Due to its significant bandwidth, an impulse radio-based multiple-access system may accommodate many users, even in multipath environments.

The effect of incoming multipath can be understood from a frequency-domain perspective by realizing that the signal bandwidth of a UWB signal is similar to the coherence bandwidth of the multipath channel with a flat response of amplitude fading at all frequencies. UWB technology's strong resolution capability also improves the performance of the radio by allowing the different multipath components to be resolved.

In a multipath environment because of huge transmission bandwidth, fine resolution of multipath arrivals is achieved leading to reduced fading for each path because the transmitted data is in the form of pulses, significant overlap is prevented and thus reducing the possibility of destructive combining.

2.1.5 Regulatory Issues

UWB has been regulated by regional regulatory bodies like FCC since its operating band has other legacy systems that are already installed worldwide like the UNII band, where many other wireless systems like 802.11a; Cordless phones etc., are already operational. These regulatory bodies tend to protect sensitive systems like GPS, federal aviation systems, etc., and also make sure UWB co-exists with existing radio services without causing much interference to these wireless systems.

In the USA, the FCC limits ensure that the UWB emission levels are exceedingly small around or lower than the spurious emission limits for all radios. For this reason, UWB is more suitable for indoor applications rather than a metro area network that spans a huge geographic area. UWB has been typically used for many years in the Ground Penetrating Radar (GPR) applications. Part - 15 rules of the FCC mandate the UWB emissions to be less than -42.3dBm/MHz. These rules guarantee significant protection for sensitive systems that include GPS, Federal aviation systems, etc. operating in the 3.1 to 10.6 GHz band.

These emissions limits are the lowest limits FCC has ever given to any other transmission technology. The FCC rules also incorporate NTIA recommendations and also made sure that the UWB technology can coexist with existing radio services with the least amount of interference.

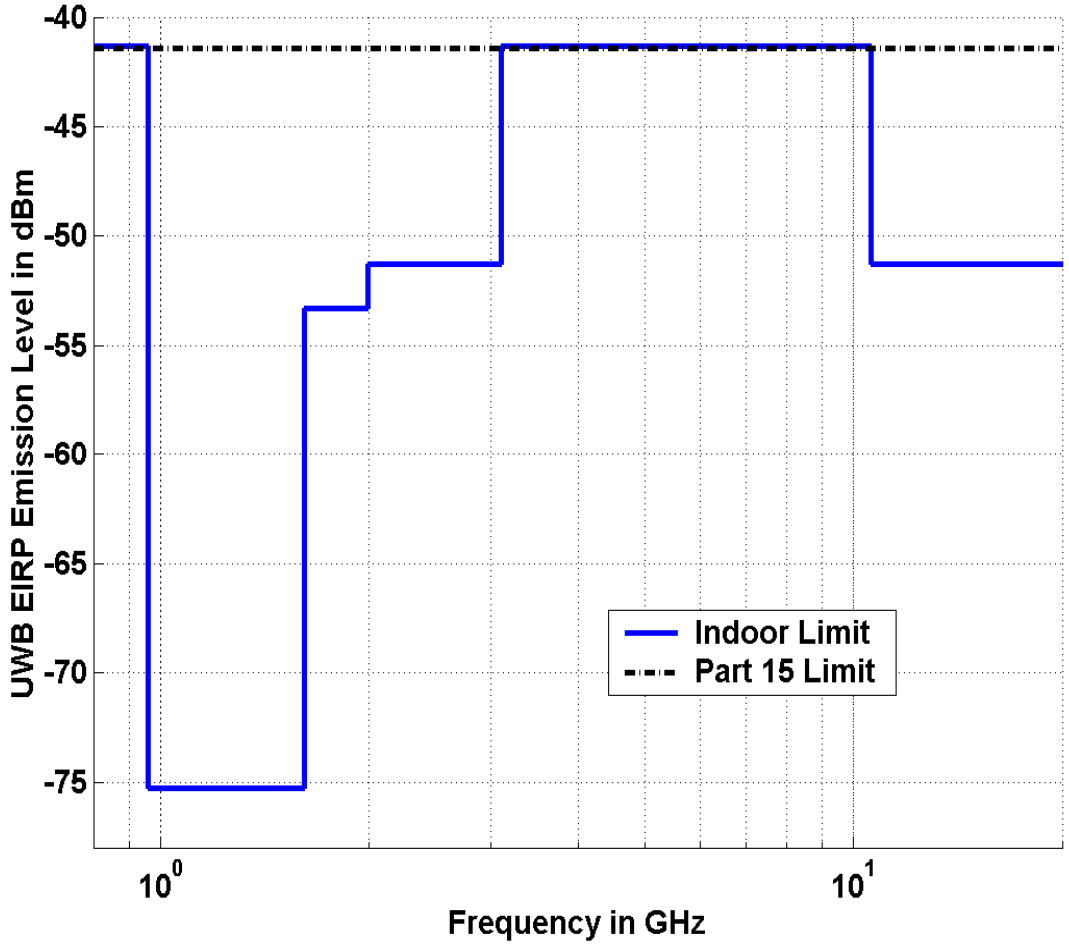

Figure 2.3: FCC Limits for Indoor Propagation of UWB

Also, these FCC limits, as shown in Figure 2.3, ensure that UWB emission levels are exceedingly small at or below spurious emission limits for all radios and at or below unintentional emitter limits of radios. These part 15 limits equate to about -41.25 dBm/MHz. When compared with the ISM band at 2.4 GHz and the U-NII bands at 5 GHz, the limits are at least 40dB more than the UWB limits per MHz.

2.1.6 Pulse Shaping

The goal of pulse shaping is to meet an arbitrary spectrum mask like the mask mandated by FCC for UWB emissions. Also, these techniques can be tuned to reduce the interference with existing wireless systems like Bluetooth (802.15.1) and 802.11a systems operating in the same band of UWB. While few of these interference sources are at one frequency, most of them have variable center frequencies like Bluetooth that uses frequency hopping techniques thus complicating the interference issues and imposing some design challenges. [9] proposes a pulse shaping filter design technique that not only satisfies the FCC spectral masks but also suppresses the Multiple Access Interference. Also, it discusses about the pulse shaping optimizer to maximize SNR.

2.2 Energy Collection Receivers

The receiver implemented in this work is based on the non-coherent energy collection receiver as discussed in [6]. The receiver utilizes *N* parallel integrators spaced equally along the symbol period and detects the energy collected in these integrators for each bit decoded in *N* time slots.

$$D_m = \int_{t_s+mT_b/N}^{t_s+(m+1)T_b/N} \left(S_r(t)\right)^2 dt \qquad (6)$$

In the above equation (6), t_s represents the starting time of the first integrator. The integrator value reflects the energy of the signal collected in the time slot of the

integrator. The receiver chooses the integrator with the maximum value which indicates the maximum energy collected in the time interval. The synchronization time t_s is given by the delay which leads to the maximum information signal energy collection, collected in the integrators, whose width is greater the symbol time of the incoming data. The width of the integrator can be an important aspect and is further discussed in chapter 4.

2.3 Synchronization in IR UWB Receivers

Synchronization can be achieved in Impulse Radio systems using the energy collection receivers discussed above. The energy is collected in the bank of parallel integrators that are equally spaced along the symbol period. A parallel search is made with the incoming data and finding the maximum output at these integrators will give the synchronization instant.

This can be achieved by sending an N bit preamble that consists of some combination of zeros or ones. When the energy collection receiver senses the reception, it clocks the integrators to start collecting the energy. After the transmitter has sent the preamble bits, the receiver calculates the maximum energy collected in these integrators and chooses the synchronization point for the incoming data stream.

The starting time of the n^{th} integrator is given by equation (7) as shown below:

$$t_n = t_1 + (n-1)T_b / N \qquad (7)$$

Where t_1 is the starting instant of the first integrator,

N is the number of integrators that are equally spaced in the symbol period.

T_b is the symbol interval.

The length of the preamble and the number of integrators can be varied for better precision of the synchronization instant. Once the synchronization instant is found, the receiver will use the output of the integrator with maximum energy in decoding the data burst until the next synchronization is performed on the incoming data.

2.4 Ideal Synchronization Scheme – Noiseless Case

An ideal synchronization scheme consists of no noise and perfect synchronization but this is impossible to achieve in wireless channels. The effect of noise and the synchronization error play an important role in the synchronization of impulse based UWB pulses. In an ideal synchronization scheme with no noise, always the integrator with the highest energy gives the correct synchronization instant. This is not true when noise is added to the received signal and when the SNR is below a certain threshold. The equally spaced parallel integrators are fed with the preamble data for collecting the energy of these pulses and, at the end of preamble, the integrator that contains the maximum energy will be the correct synchronization instant with an error equal to half the distance between two adjacent integrators. The proposed algorithm works well when the SNR is above a certain

threshold level. This threshold level varies for different channel models and is detailed in chapter 4.

Probability of False Alarm is one way to quantify the significance of the proposed algorithm for synchronization. Higher SNR signals have a low probability of false alarm and lower SNR signals have a higher probability of false alarm as will be seen later. The probability of false alarm for an ideal case will be zero as the algorithm correctly chooses the integrator with the maximum energy. Figure 2.4 shows the ideal noiseless pulses at the receiver in both time domain and frequency domain.

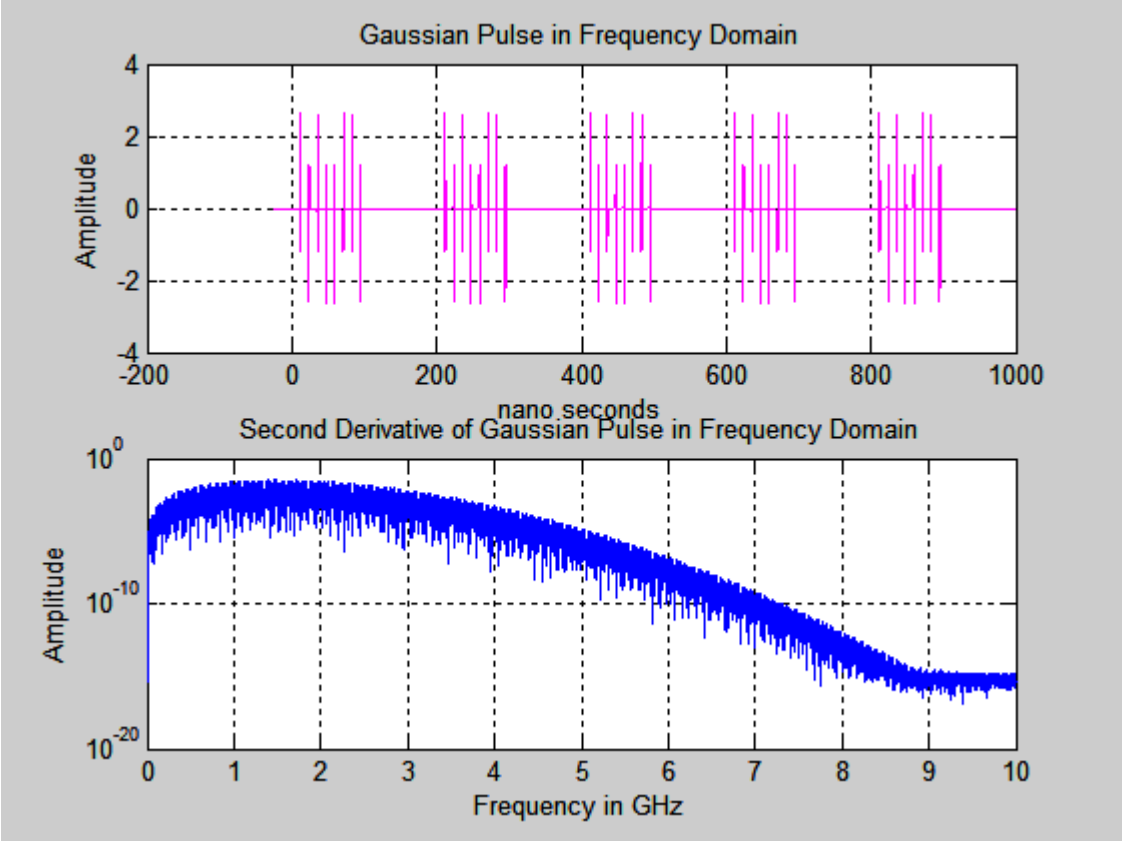

Figure 2.4: Ideal Case (Noiseless)

2.5 Effects of Noise on the Synchronization Scheme

Noise in communication systems plays a major role in the design of any radio. As discussed above, the noise in the channel might signal a false alarm for the proposed algorithm when the received SNR is below a certain threshold. The probability of false alarm for synchronization is low for high SNR and vice versa.

An ideal synchronization scheme consisting of no noise is shown in Figure 2.5. It is very easy to find the synchronization instant with the bank of integrators that span the symbol time. The integrator with maximum amount of energy gives the correct synchronization instant with an error equal to half the spacing between the integrators.

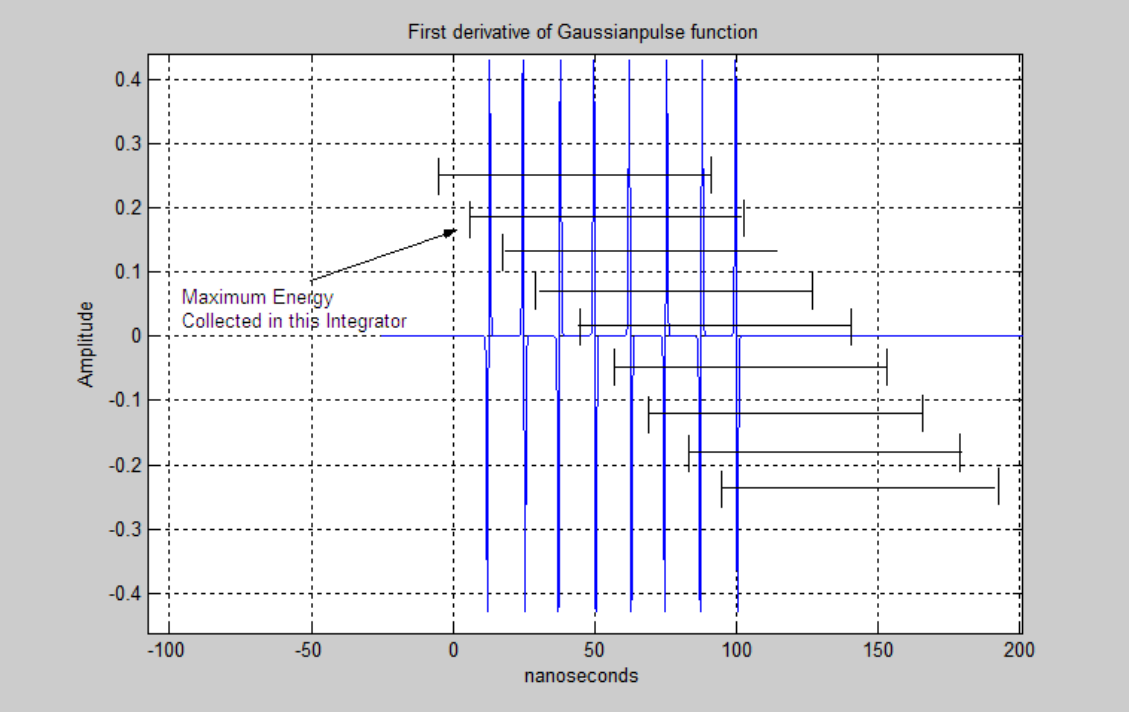

Figure 2.5: Parallel Bank of Integrators for Synchronization

Figure 2.6 shows the typical received UWB waveform at the receiver in the presence of noise.

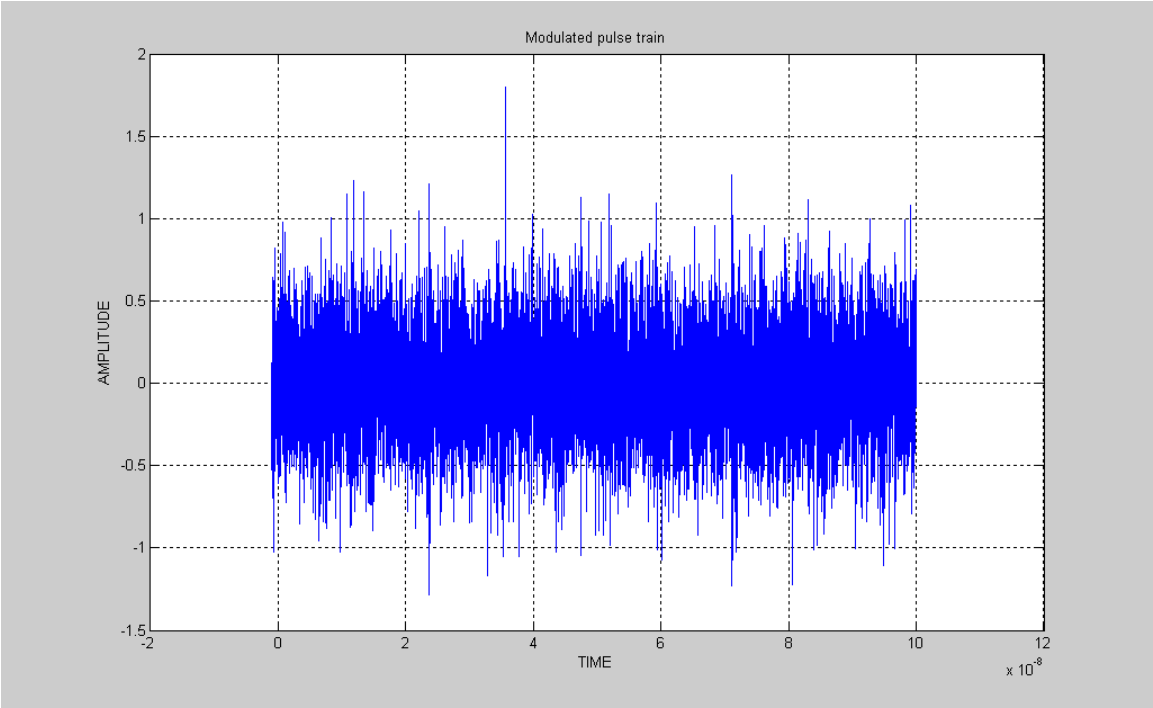

Figure 2.6: Noisy UWB Waveform at the Receiver.

Once noise is added, the contribution of noise energy to the integrators may not yield the synchronization instant correctly because of its random behavior. Noise power is defined as the sum of thermal noise power at the input of the system, gain of the system and the Noise Figure. Thermal Noise Power at the input of the system is given by equation (8):

$$N_{thermal} = KTB \qquad (8)$$

Where

$N_{thermal}$ is the Thermal noise power at the input of the system.

K is the Boltzmann constant and is equal to $1.38*10^{-3}K^{-1}$

T is the ambient Temperature in Kelvin and

B is the bandwidth of the system in Hz.

The total Noise Power at the output is given by equation (9).

$$N_{Output}\ (dBm) = N_{Thermal} + G + NF \qquad (9)$$

Where

N_{Output} is the total output noise power.

$N_{Thermal}$ is the Thermal noise at the input of the receiver as calculated by (8)

G is the system gain.

NF is the total Noise Figure of the system.

Thermal noise is significantly higher in UWB systems because of the higher bandwidth associated with UWB pulses (KTB). The problem is worsened if there is any narrowband signal that appears as noise to this integrator. For example, an 802.11a system that operates at 5.8GHz may add significant amount of noise to a portion of the preamble time period making the integrator that captures this interference as the integrator with maximum energy and wrongly determining the synchronization instant.

2.6 Conclusion

From the above, we can see the following:

1. Energy collection receivers are very simple to implement in the case of Impulse Radio UWB systems without using energy consuming components.
2. Synchronization, one of the important aspects of impulse radio, can be done using energy collection receivers using a bank of integrators spaced equally along the symbol period.
3. Noise is a major factor that can affect the accuracy of algorithm.
4. Probability of False Alarm for synchronization is used to signify the veracity of the proposed algorithm in the presence of noise.

Chapter 3

Channel Models for Ultra WideBand Systems

The presence of multiple path components in an indoor environment complicates the modeling of the channel and receiver structures for narrow pulse based systems like UWB. The channel model has to take into account the time varying properties of the multiple path signals at the receiver. The channel model used for evaluating the synchronization algorithm is the modified Saleh Valenzuela channel model proposed by the Channel-Modeling sub-committee of study group IEEE 802.15.3a. [4] This chapter provides in-depth analysis of the modified SV model proposed for wireless personal area networks.

3.1 Modified Saleh Valenzuela Channel Model

The original model proposed by Saleh and Valenzuela is based on the empirical measurements carried out in indoor environments in 1987. The time of arrival of clusters is modeled as a Poisson arrival process with rate Λ, [11] as shown in equation (10).

$$p\left(T_n / T_{n-1}\right) = \Lambda e^{-\Lambda(T_n - T_{n-1})} \qquad (10)$$

Where T_n and T_{n-1} are the times of arrival of n^{th} and the $(n-1)^{th}$ clusters.

Also, within each cluster, the multipath contributions arrive according to a Poisson process with rate λ as shown in equation (11) below.

$$p\left(\tau_{nk} / \tau_{(n-1)k}\right) = \lambda e^{-\lambda(\tau_{nk} - \tau_{(n-1)k})} \qquad (11)$$

Where τ_{nk} and $\tau_{(n-1)k}$ are the time of arrival of the n^{th} and $(n-1)^{th}$ contributions within cluster k. The time of arrival within each cluster, $\tau_{n1,}$ for n=1, 2 ….N is set to 0.

The original model proposed by Saleh and Valenzuela assumes the multipath gain magnitude as statistically independent and Rayleigh distributed positive random variables, while the phase values are assumed to be statistically independent uniform random variables over [0,2π). The average power delay profile is characterized by an exponential decay of the amplitude of the clusters, and a different exponential decay for the amplitude of the received pulses inside each of these clusters.

The channel model proposed by IEEE 802.15.3a uses a similar channel model and to better fit the observed data, a few modifications to the S-V model has been proposed. A log normal distribution of the multipath gain magnitude is proposed instead of the Rayleigh distribution and an additional log-normal variable was suggested for representing the variations of the total multi-path gain, and, the phase of the channel impulse response is modeled as either 0 or π. The discrete time multipath channel impulse response initially proposed by Foerster (2003), is given in equation (12) below.

$$h(t) = X \sum_{n=1}^{N} \sum_{k=1}^{K(n)} \alpha_{nk} \delta(t - T_n - \tau_{nk}) \qquad (12)$$

Where

X = log normal random variable representing the amplitude gain of the channel;

N = number of clusters;

K(n) = number of multi-path contributions within n^{th} cluster;

α_{nk} = coefficient of the k^{th} multipath contribution of the n^{th} cluster;

T_n = time of arrival of the nth cluster;

τ_{nk} = delay of the k^{th} multipath contribution within the n^{th} cluster.

The channel coefficient, $\alpha_{nk,}$ is defined as:

$$\alpha_{nk} = p_{nk} \beta_{nk} \qquad (13)$$

Where p_{nk} = discrete random variable assuming equi-probable values of +1 or -1

β_{nk} is the log normal distributed channel coefficient from k^{th} multipath contribution and n^{th} cluster. This can be expressed as shown in equation (14).

$$\beta_{nk} = 10^{x_{nk}/20} \qquad (14)$$

where x_{nk} is assumed to be a Gaussian random variable with mean μ_{nk} and standard deviation, σ_{nk}. x_{nk} can be defined as follows:

$$x_{nk} = \mu_{nk} + \xi_n + \zeta_{nk} \qquad (15)$$

Where ξ_{nk} and ζ_{nk} are two independent Gaussian random variables representing the fluctuations of the channel coefficient on each cluster and on each contribution, respectively.

Also, from the modified S-V model, the arrival time variables, T_{nk}, τ_{nk} are assumed to be two Poisson distributed variables with average rates Λ and γ respectively..

The amplitude gain X is assumed to be a log normal distributed random variable.

$$X = 10^{g/20} \qquad (16)$$

Where g = Gaussian random variable with mean g_0 and variance σ_g^2.

g_0 depends on the average total multipath gain G, which is measured at the location under examination and is quantified as shown in equation (17).

$$g_0 = \frac{10\ln G}{\ln 10} - \frac{\sigma_g^2 \ln 10}{20} \qquad (17)$$

Where g_0 = Mean of the Gaussian random variable g;

G = total multipath gain;

σ_g^2 = Variance of the variable g.

From the above equations, the channel is fully characterized after defining the following parameters:

1. The cluster average arrival rate Λ.
2. The pulse average arrival rate λ.
3. The power decay factor Γ for all the clusters.
4. The power decay factor γ for pulses within a cluster.
5. The standard deviation σ_ξ of the variations of the channel coefficients for clusters.
6. The standard deviation σ_ζ of the variations of the channel coefficients for pulses within each cluster.
7. The standard deviation σ_g of the channel amplitude gain.

Modified S-V model Parameters

The initial set of values has been suggested by the IEEE Channel modeling committee as shown in Table 1. The list is designed for various channel conditions listed below:

1. CM1: LOS (Line of Sight) from 0-4m distance.
2. CM2: NLOS (Non Line of Sight) from 0-4m distance.
3. CM3: NLOS from 4-10m distance.
4. CM4: Extreme NLOS channel conditions from 4-10m distance.

Scenario	Λ (ns^{-1})	λ(ns^{-1})	Γ	γ	σ_ξ(dB)	σ_ζ(dB)	σ_g(dB)
CM1 LOS (0-4m)	0.0233	2.5	7.1	4.3	3.3941	3.3941	3
CM2 NLOS (0-4m)	0.4	0.5	5.5	6.7	3.3941	3.3941	3
CM3 NLOS (4-10m)	0.0667	2.1	14	7.9	3.3941	3.3941	3
CM4 Extreme NLOS (4-10m)	0.0667	2.1	24	12	3.3941	3.3941	3

Table 1: IEEE UWB Channel Parameters

3.1.1 Channel Model 1 (CM1)

The channel model 1 (CM1) deals with the channel characteristics within 4m range of the UWB nodes in a Line of Sight (LOS) environment. In this model, the first component received is the strongest followed by multipath components with diminishing amplitudes. The channel impulse response for this case is shown in Figure 3.1. Maximum energy is collected in the first few pulses as shown in Figure 2.5.

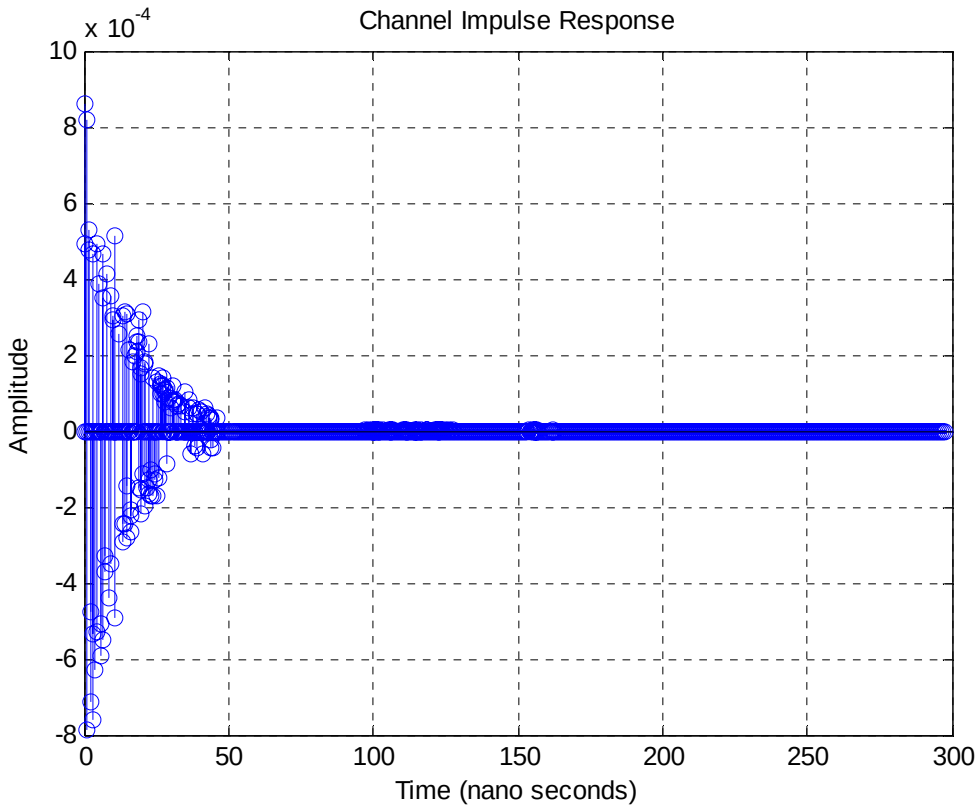

Figure 3.1: Channel Impulse Response for CM 1

3.1.2 Channel Model 2 (CM2)

The channel model 2 (CM2) deals with the channel characteristics within 4m range of the of the transmitter and receiver in a Non Line of Sight (NLOS) environment. The channel impulse response for this case is shown in Figure 3.2. From the figure, we observe that the strongest peak is not the first component reaching the receiver which is typical of a NLOS channel where obstacles are located in the path of the transmission channel. The strongest peaks reach the receiver after reflections and diffractions while the first

component to reach the receiver is the one that penetrates these obstacles after undergoing heavy attenuation.

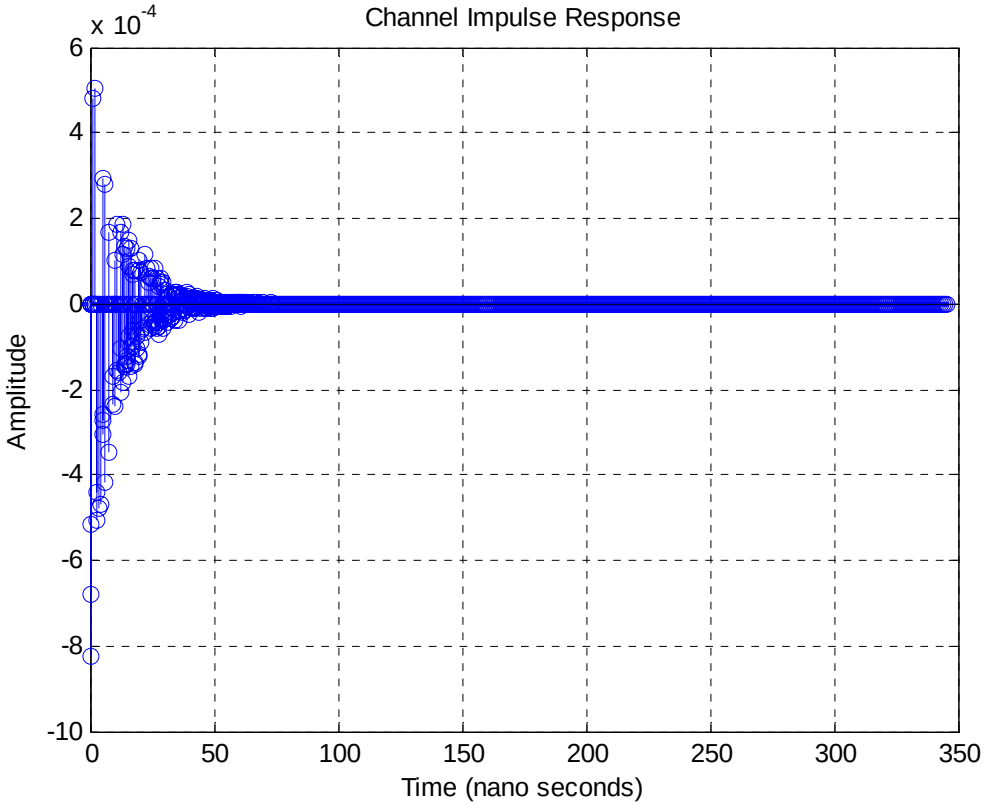

Figure 3.2: Channel Impulse Response for CM2

3.1.3 Channel Model 3 (CM3)

The channel model 3 (CM3) deals with the channel characteristics from 4m to 10m range of the UWB nodes in a Non Line of Sight (NLOS) environment. The channel impulse response for this case is shown in Figure 3.3. The pulses are received for a much longer period than in cases 1 and 2. Also, the impulses are characterized by higher temporal dispersion of the energy than in cases 1 and 2.

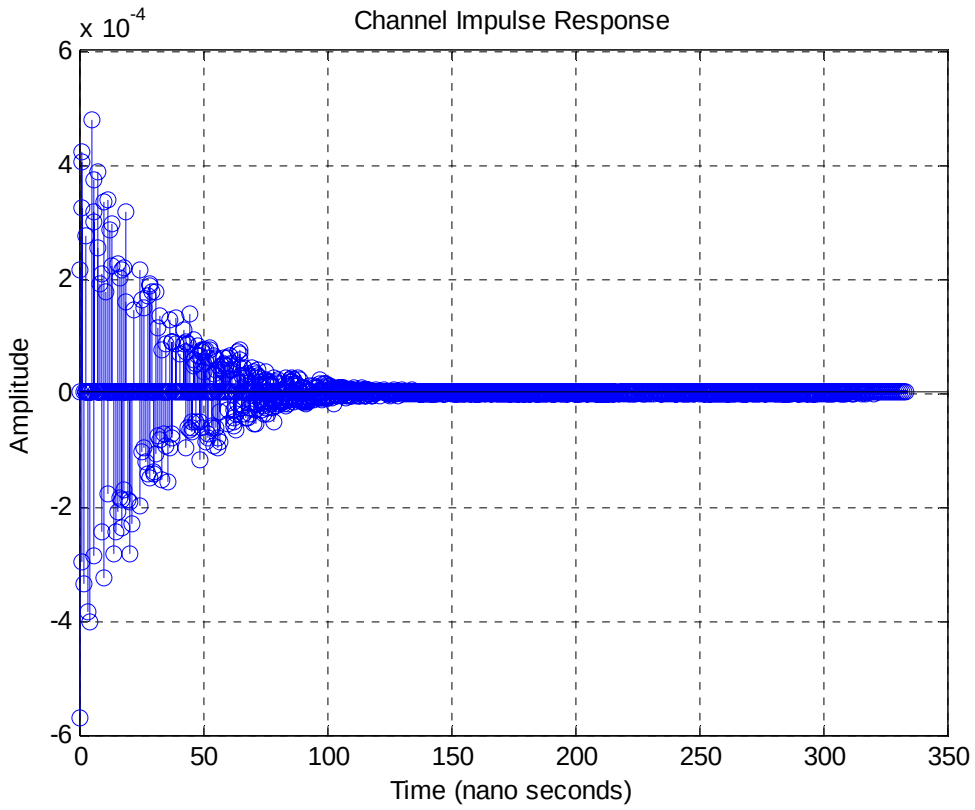

Figure 3.3: Channel Impulse Response for CM3

3.1.4 Channel Model 4 (CM4)

The channel model 4 (CM4) deals with the channel characteristics in an extreme NLOS characteristics when the distance between the transmitter and the receiver is from 4m to 10m. This is the case where the channel is heavily polluted with multi path components and noise. The channel impulse response for this case is shown in Figure 3.4. From the figure, we observe that there are many multipath components than the previous cases. The energy of the pulses is received even after 150ns. The receiver should collect all the energy before deciding on the transmitted data.

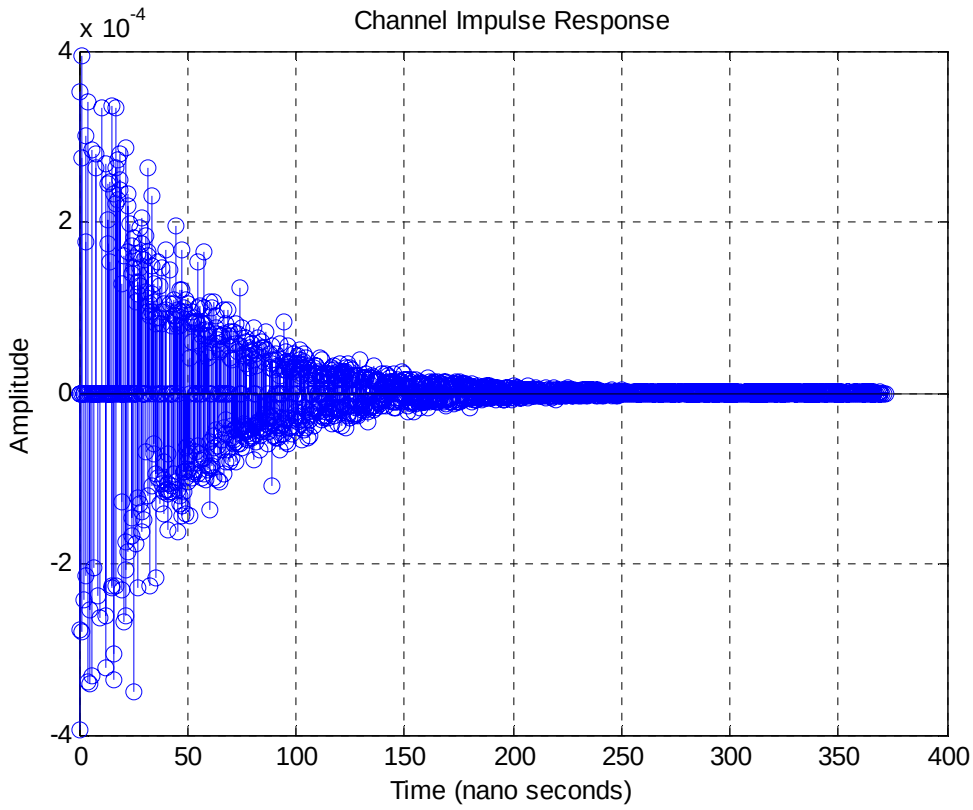

Figure 3.4: Channel Impulse Response for CM4

The important aspect of non linear energy collection receivers is to choose the integration window that satisfies all the channel models described without overkill. The length of the integrator should be at least the length of the channel impulse response to collect all the information from multipath components. This is discussed in detail in chapter 4 including the simulation details.

Chapter 4

Simulation Details of the Synchronization Scheme

This chapter provides in-depth analysis of the synchronization algorithm and the details of the simulation performed to characterize the performance of the energy collection receivers. Probability of Detection and the Probability of False Alarm for synchronization under various channel conditions are studied. The effect of the length of the integrator on the performance of this receiver is also studied.

4.1 Details of the Synchronization Algorithm

This analysis is the extension of the work from [6]. The results from this analysis show the importance of synchronization in UWB systems and the effects of synchronization in presence of noise for various use cases. The synchronization algorithm is based on the energy collection process at the input of the receiver.

During the initial tracking phase of the receiver, the transmitter is chosen to send a preamble with a specified number of zeros until the receiver is synchronized to the transmitter. At the receiver, there is a parallel bank of equally spaced overlapping integrators to collect the energy from the bits sent by the transmitter in determining the

synchronization instant. The preamble chosen is a predetermined number of continuous zeroes. The number of zeroes is chosen to be 5 as shown in Figure 4.5. The cases considered here involve PPM for single user scenario under various channel conditions of the modified Saleh-Valenzuela model.

The transmitted signal of a PPM based UWB signal is represented as shown in equation (18) below:

$$s(t) = \sum_{k=-\infty}^{\infty} w_{tr}(t - kT_b - jT_c - T_s d_k)(c_p)_j \qquad (18)$$

Where $w_{tr}(t)$ is the transmitted pulse waveform with pulse width T_p [10].

T_b is the symbol interval.

T_s is the time shift used to distinguish different symbols and

d_k is the k^{th} transmitted symbol given by $d_k \in [0,1,....M-1]$

$T_c = NT_p$ where N is the chip interval.

$(c_p)_j$ is the j^{th} chip of the pseudo-random (PR) code which is either a -1 or a 1.

$R_d = 1/T_b$ is the data rate.

The received signal for this signal is described by equation (19) as described below:

$$s_r(t) = \sum_{l=0}^{L} A_i \sum_{k=-\infty}^{\infty} \sum_{j=1}^{N} w_{rx}(t - kT_b - jT_c - T_s d_k - \tau_l)(c_p)_j + n(t) \qquad (19)$$

Where $w_{rx}(t)$ is the received signal and the first derivative of $w_{tx}(t)$ as the UWB antenna acts as a differentiator[7]. L is the number of resolvable paths, A_i is the gain for path i and $n(t)$ is the zero mean additive Gaussian noise.

The values used in the simulation are:

T_b = 1500ns and hence the data rate R_b = 0.66Mbps.

N = 5 pulses per bit.

Pulse Width T_p = 0.5ns.

Distance between two integrators = 10ns.

Number of Integrators = 4.

Length of integrator = 250ns.

The code word (PN Sequence) chosen for each bit is: c_j = [1,-1,1,-1,-1,1,1,-1].

The UWB waveform $w_{tx}(t)$ used here is the first derivative of Guassian pulse and $w_{rx}(t)$ is the second derivative of Gaussian pulse because of it special properties that can be applied to impulse based UWB systems. The channel models used in the simulation are the modified Saleh Valenzuela models proposed by the channel modeling committee of IEEE 802.15.3a [11].

The series of pulses are positioned according to the user's data bit that is to be transmitted. These pulses are multiplied by the orthogonal PN sequence. A Gaussian duo

pulse (second derivative of Gaussian pulse) is considered here for the special characteristics it possesses as described in [7]. Each bit is represented by the series of pulses multiplied by the PN sequence. The modulation employed is called Bit Position Modulation. If the pulses appear in the former part of the time period, the bit transmitted is a '0' and if the pulses appear in the latter part of the time period, the bit transmitted is a '1' as the pulses are multiplied by the delay element according to equation (19). These pulses are shown in Figure 4.1 and 4.2 for transmission of a '0' and a '1' respectively.

In the figure shown below,

T_s = 15ns.

$T_b = 10T_s$ = 1500ns.

N = 5 pulses per bit.

The value of T_b is chosen to be 1500ns. The time interval is chosen to be ten times T_s. The multiple of this value can be changed to accommodate different data rates. For example, if the multiple is chosen to be 4, then $T_b = 4T_s$ = 60ns. This results in a data rate of $R_b = 1/T_b$ = 16Mbps. For the simulations, T_b is chosen to be $10*T_s$ resulting in a data rate of 0.66Mbps.

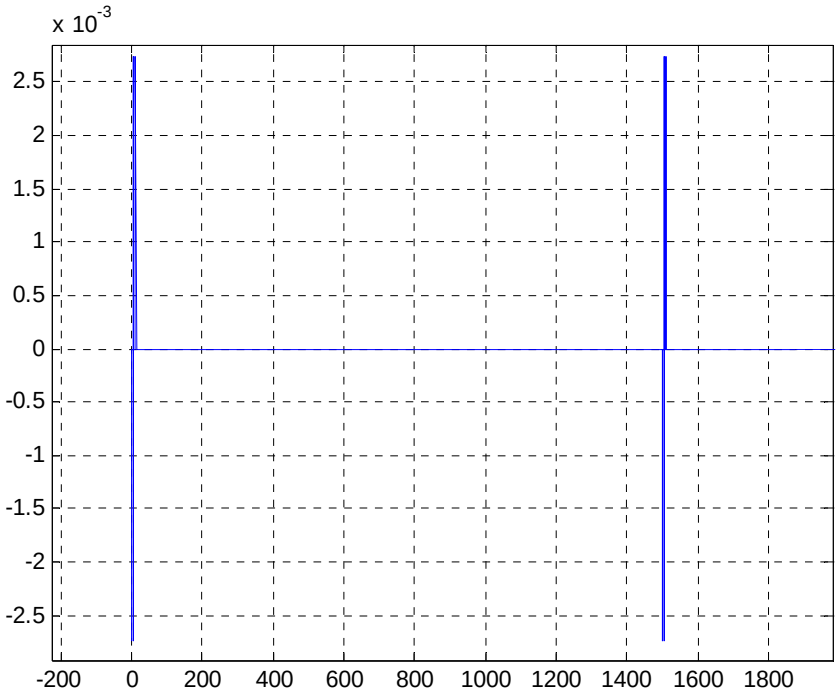

Figure 4.1: Pulses Transmitted as '0's.

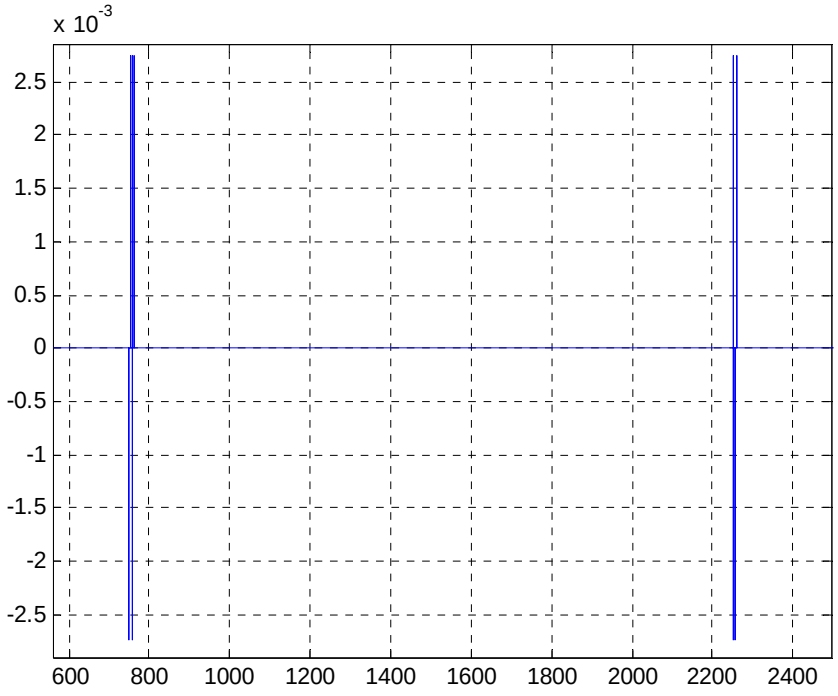

Figure 4.2: Pulses Transmitted as '1's.

As shown in the Figures 4.1 and 4.2, if the bit to be transmitted is a '0', it is transmitted in the former part of the symbol interval, T_b, from 0 to 15ns and if the transmitted bit is a '1', it is transmitted in the latter part of the symbol interval from 750ns to 765ns. The receiver consists of a series of integrators spaced evenly within the symbol period. Each of these integrators has a window size equal to 250ns enough to capture the energy of all the pulses. The length of the integrator is very important to capture all the energy from all the multipath components. This is studied in more detail in section 4.7. The number 250ns is chosen from the impulse response graphs of figures 3.2, 3.3, 3.4 and 3.5. to accommodate the whole multipath energy for all the channel conditions. Figure 3.5 shows that CM4 has the largest amount of time dispersion of about 225ns. Hence the integration interval is chosen to be little greater than 225ns.The number of integrators used for energy collection can be varied according to the complexity of the receiver. Once the receiver starts receiving the pulses of the preamble, the integrators start to load and the energy is collected in these integrators. After the time equal to the pre-determined number of preamble bits has elapsed, the synchronization instant is given by the integrator which represents the maximum energy collected.

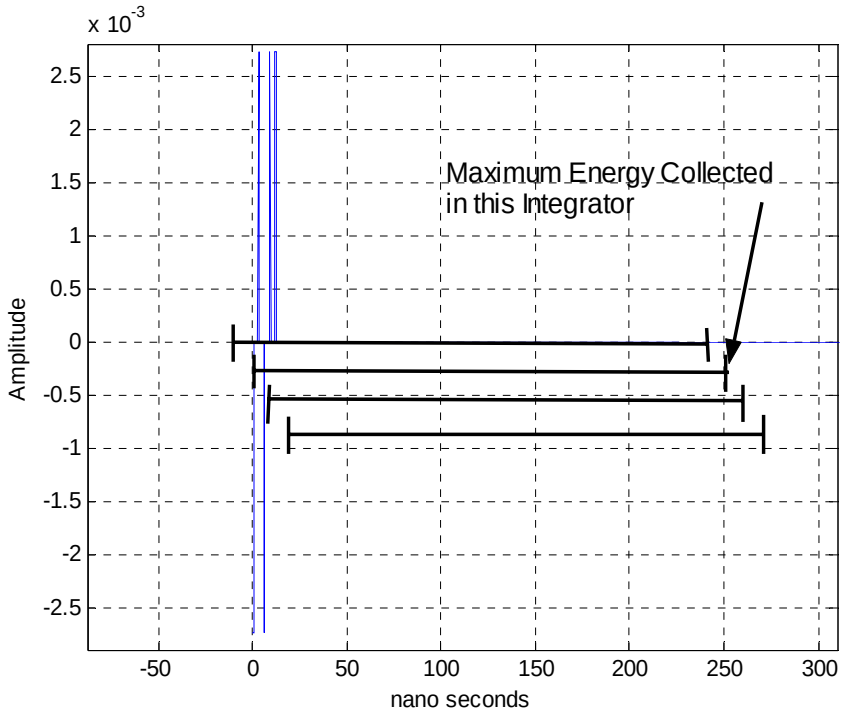

Figure 4.3: Bank of Integrators Spanning the Symbol Time

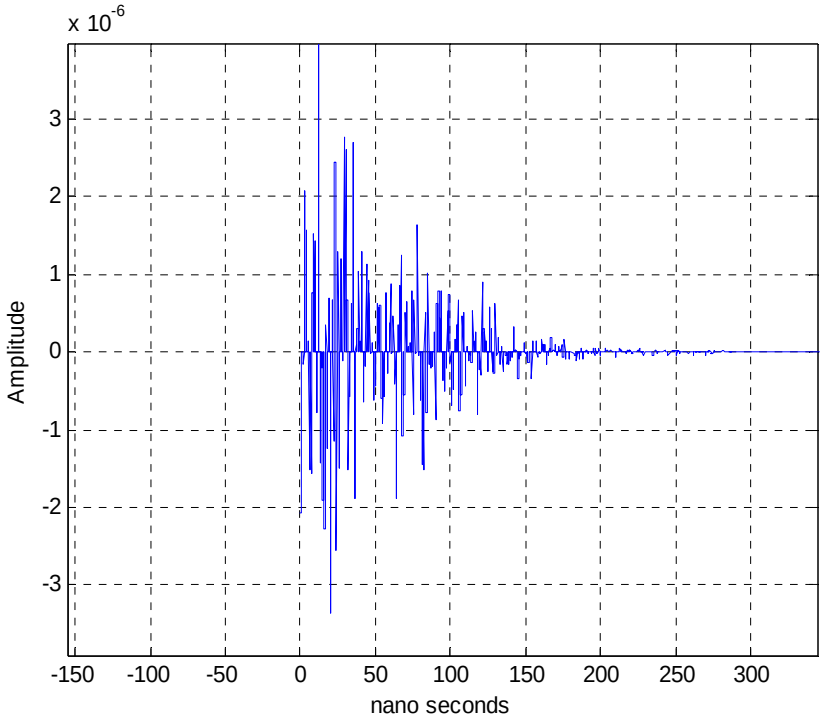

Figure 4.4: Noise and Multipath Signal

From Figure 4.3, we can see the second integrator is arranged to span the entire pulses inside its integrator window including the multipath energy. Even though the first integrator spans all the pulses, it fails to collect the entire multipath energy from the pulses as can be seen from the noise and multipath polluted signal in Figure 4.4. The energy collected in these integrators is the square of the time domain waveform. Hence in the ideal case, with no noise and multipath components, and when the length of the integrator is equal to $T_{s,}$ the second integrator will give the approximate of the synchronization instant for decoding the UWB pulses.

The separation between adjacent integrators is chosen to be 10ns in the simulation. The total number of integrators chosen is 4. This number can also be increased for more precise synchronization instant. The maximum error in determining the synchronization instant is half the distance between two adjacent integrators and hence in this case, it is 10/2 = 5ns.

The following use cases have been studied in this work.

1. Case 1 (LOS 0 - 4m).
2. Case 2 (NLOS 0 - 4m).
3. Case 3 (NLOS 4-10m).
4. Case 4 (Extreme NLOS)

4.2 Flow Chart of Algorithm

In the simulation, 500 frames of data is generated using Matlab. Each frame is composed of preamble bits and data bits as shown in Figure 4.5.

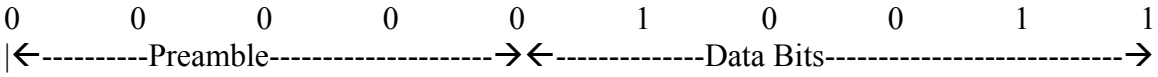

Figure 4.5: Frame Structure

Each frame consists of 10 bits where the first 5 bits correspond to preamble bits while the next 5 bits correspond to the data bits. The number of preamble bits and data bits can be optimized for each channel condition without overkill. Figure 4.6 shows the timing of the preamble pulses when $T_b = 10T_s$ = 1500ns. Figure 4.7 shows the flow chart of the Monte Carlo simulation performed on the symbol bits.

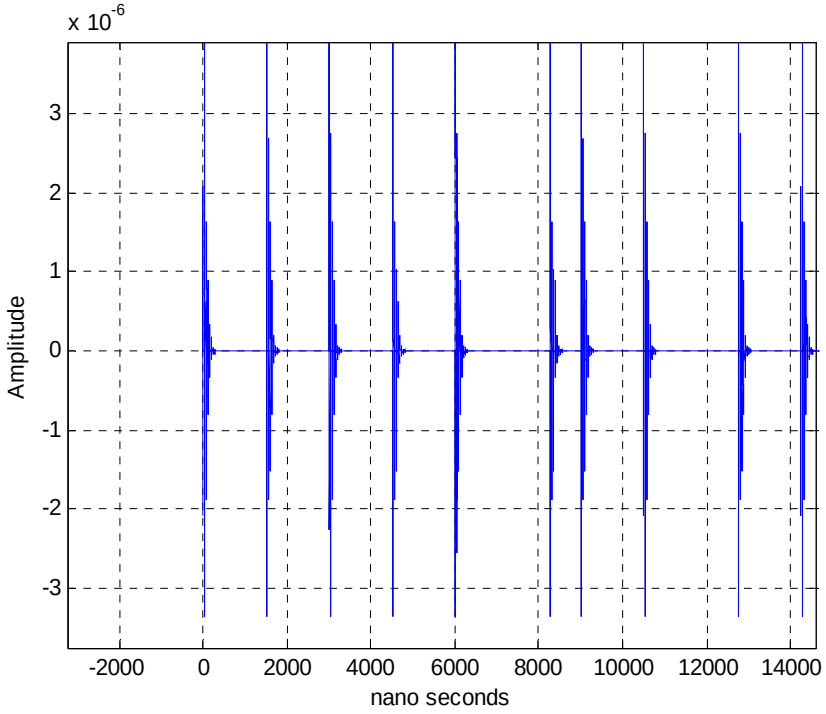

Figure 4.6: Timing of Preamble

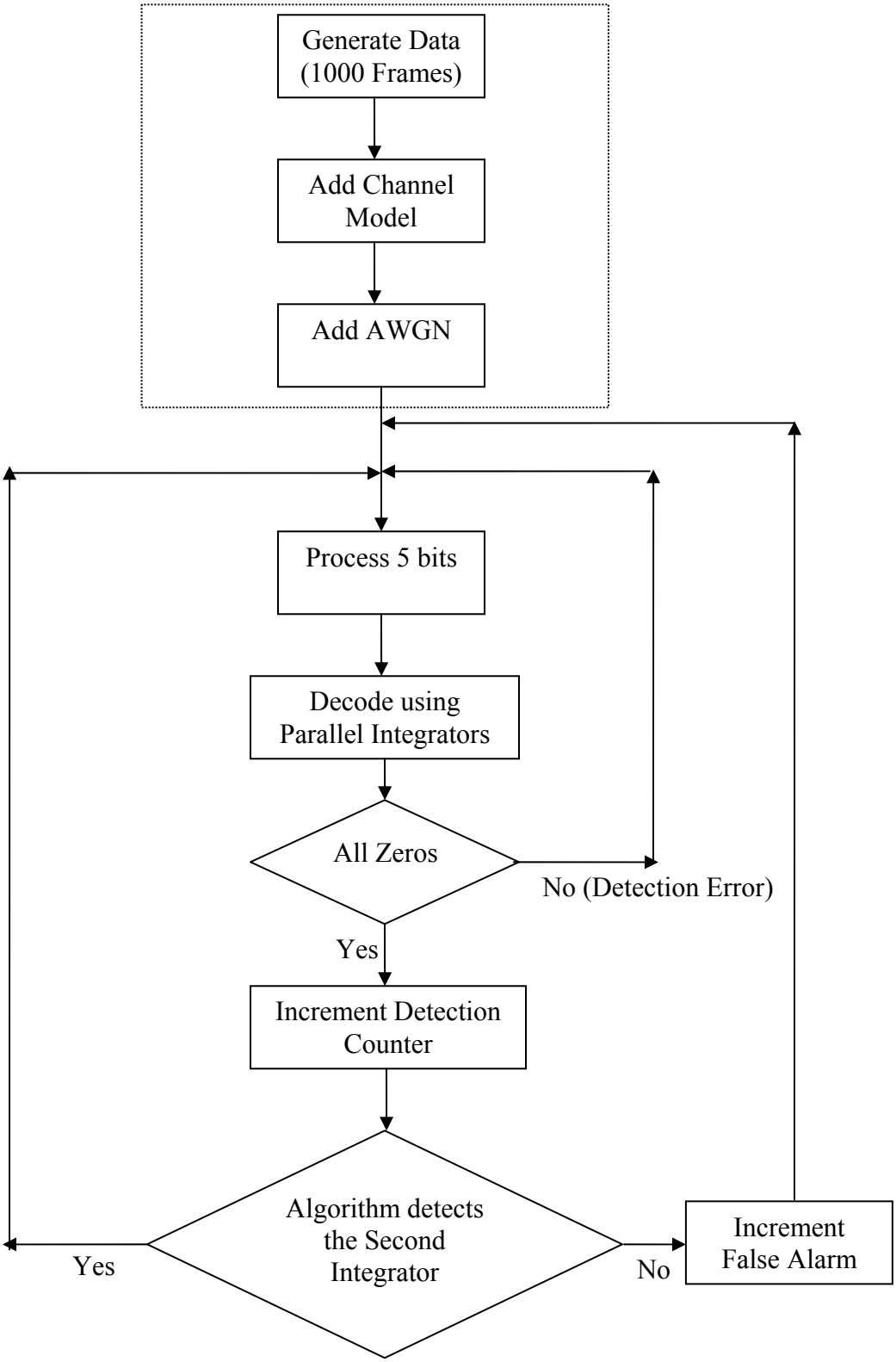

Figure 4.7: Flow Chart of Synchronization Scheme

4.3 Probability of Detection

It's a known fact that all the wireless channels are polluted with noise; the correct integrator not only captures the energy of all the pulses, but also the noise contributed by the channel. The multipath channel conditions further deteriorate the received signal leading to Inter Symbol Interference (ISI) and errors in the detection of data. Probability of detection and probability of false alarm give a measure of the performance of the synchronization algorithm studied. In the simulations performed, the second integrator is chosen to collect the energy in the correct time interval as shown in Figure 4.3.

As all the integrators give some value even if there is no transmission, because of energy collection, the algorithm has to decode few preamble sequences before signaling a detection. Care has to be taken at the transmitter using source coding such that the transmitted sequence of bits doesn't contain the preamble. Doing so will not signal a false alarm at the receiver as these bits are part of data rather than preamble. Also, the length of the integrators is adjusted such that it is long enough to capture all the data for all channel conditions. A detection is defined as decoding the preamble bits at the receiver. It is possible that the integrators signal a preamble detection due to corruption of data bits or when there are no data bits at all. Hence the receiving algorithm should make sure that there are few preamble sequences detected before detecting the data bits. For example, if the preamble bits are sent every 5ms, the receiving algorithm should also detect preamble sequences every 5ms and then call it a detection. Once the algorithm performs the detection of few preamble sequences, timing synchronization is achieved using the time

interval of the integrator that collects the maximum energy (collected from the preamble bits) for further processing of the data bits until the next synchronization phase.

4.4 Probability of False Alarm for Synchronization

A False Alarm for synchronization is signaled when the time interval of the integrator with maximum energy is not the time interval of the preamble bits transmitted. This can lead to significant bit errors during the detection process. When a false alarm happens, the penalty imposed is usually the time taken until the next synchronization or when the error detection algorithm, implemented on the data bits, signals that the data bits received are in error. Hence, it is important that there are few consecutive detections of preamble before decoding the data bits.

In the simulation, the false alarm is calculated only when there is a detection of the preamble. The performance of the algorithm is characterized by the Probability of False Alarm using Monte-Carlo simulations. The second integrator is chosen to be collecting the energy in the correct time interval as shown in Figure 4.3. Probability of False Alarm is given by equation (20).

$$P_{e\ /\ SNR\,|P_d=1} = \frac{1}{ND}\sum_{r=1}^{N} E_r \qquad (20)$$

$E_r = 1$ *if* $E_{max} \neq 2$, $E_r = 0$ *if* $E_{max} = 2$

where $E_{max} \in [E_1, E_N]$ is the *Integrator with Maximum Energy Collected* and E_n is the nth integrator, *ND* is the number of detections out of *N* symbols. Probability of False Alarm for synchronization for a given SNR is the ratio of the total number of times the algorithm fails (when the maximum energy is not collected in the second integrator) to the total number of Monte-Carlo simulations performed given that the probability of detection is 1. When the maximum energy is not collected in the second integrator, an error in the decision is said to have occurred. This is the decision threshold for the algorithm. For a given SNR, this simulation is run for 1000 symbols, each symbol containing 5 preamble bits.

The Signal to Noise Ratio is varied and the Probability of False Alarm for synchronization is studied at different SNR values for different channel models as discussed below.

4.5 Simulation with AWGN only

The probability of detection is calculated when only channel noise is added. This case doesn't include the multipath energy received during the transmission of pulses. This signifies the importance of Probability of Detection and Probability of False Alarm for synchronization in characterizing the performance of the algorithm. For this case, the first integrator is disabled because for the ideal case, both the first and the second integrators contain all the pulses. As the length of the integrators is much $10*T_{s,}$ both the first and the second integrators receive the energy from all the pulses. When the length of the

integrator is exactly equal to $T_{s,}$ only the second integrator captures all the energy of the pulses.

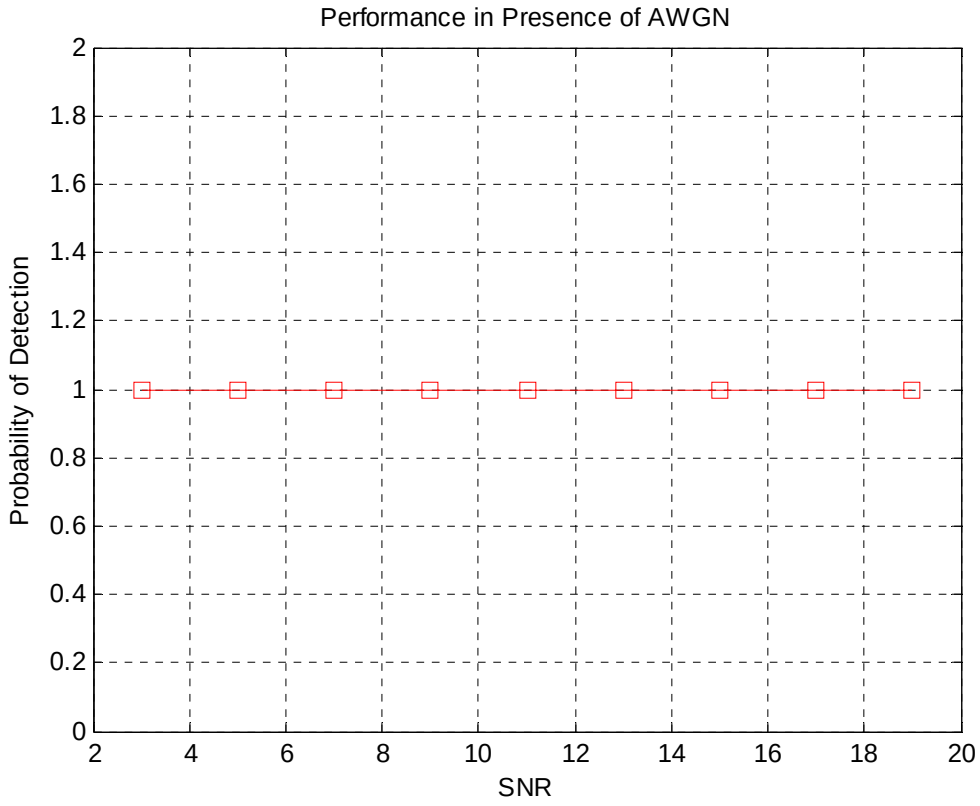

Figure 4.8: Detection vs. SNR with AWGN only

From Figure 4.8, the probability of Detection is always 1, when simulated for data containing 1000 symbols, indicating that the algorithm decodes the preamble correctly for SNR values ranging from 3 to 20dB. This case doesn't include the multipath energy received during the transmission of pulses. The Probability of False Alarm for synchronization, which is calculated only when there is a detection of preamble, is obtained to be always zero indicating that the correct integrator time interval is obtained for SNR values ranging from 3dB to 20dB. Simulations with integration window equal to

250ns, and including the first integrator resulted in the same performance as shown in figures 4.8 and 4.9.

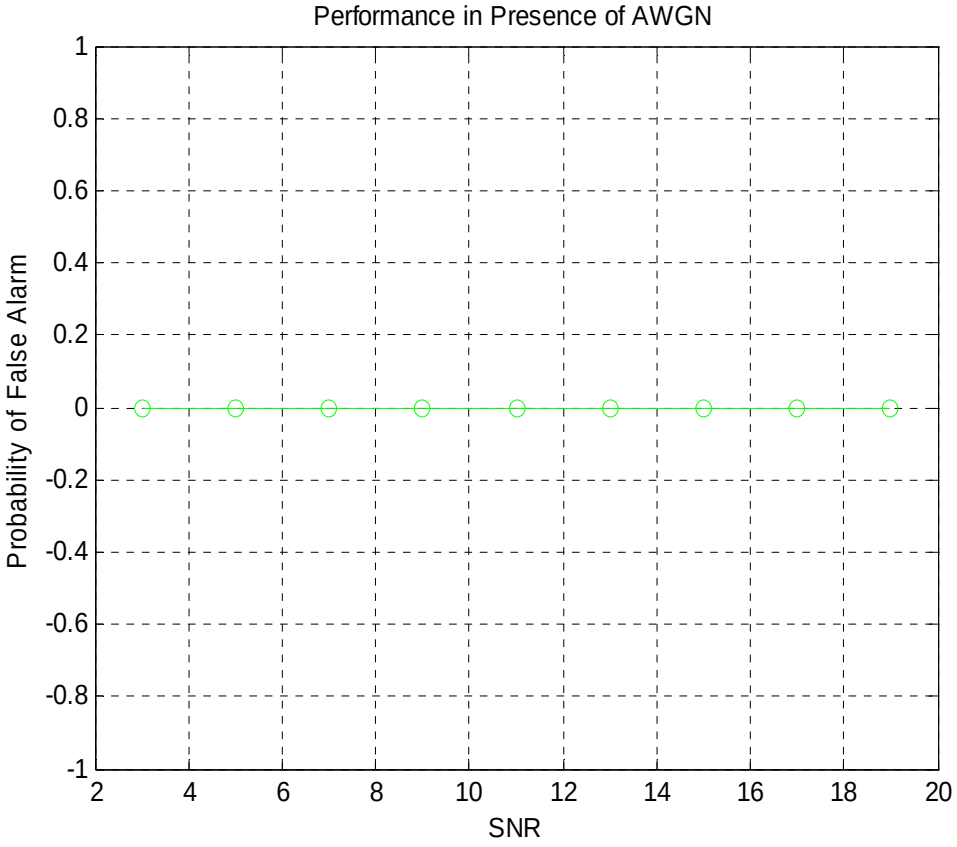

Figure 4.9: False Alarm vs. SNR with AWGN only

4.6 Simulation with Channel Model and AWGN

This section describes the simulation details involved using various channel conditions and AWGN. As described in section 3.1, the channel model considered for UWB is the modified Saleh Valenzuela model under various conditions. The following cases have been simulated as part of this work:

- Case 1 (LOS 0-4m)
- Case 2 (NLOS 0-4m)
- Case 3 (NLOS 4-10m)
- Case 4 (Extreme NLOS)

4.6.1 Case 1 (LOS 0-4m)

Case 1 deals with the Line of Sight channel modeling where the distance between the UWB nodes is less than 4m and having a direct line of sight. This is the case where the first multipath component's energy is higher than subsequent multipath components bounced off from obstacles because of the line of sight component. Figure 4.10 shows the graph of Probability of Detection vs. SNR and figure 4.11 shows the graph of Probability of False Alarm vs. SNR.

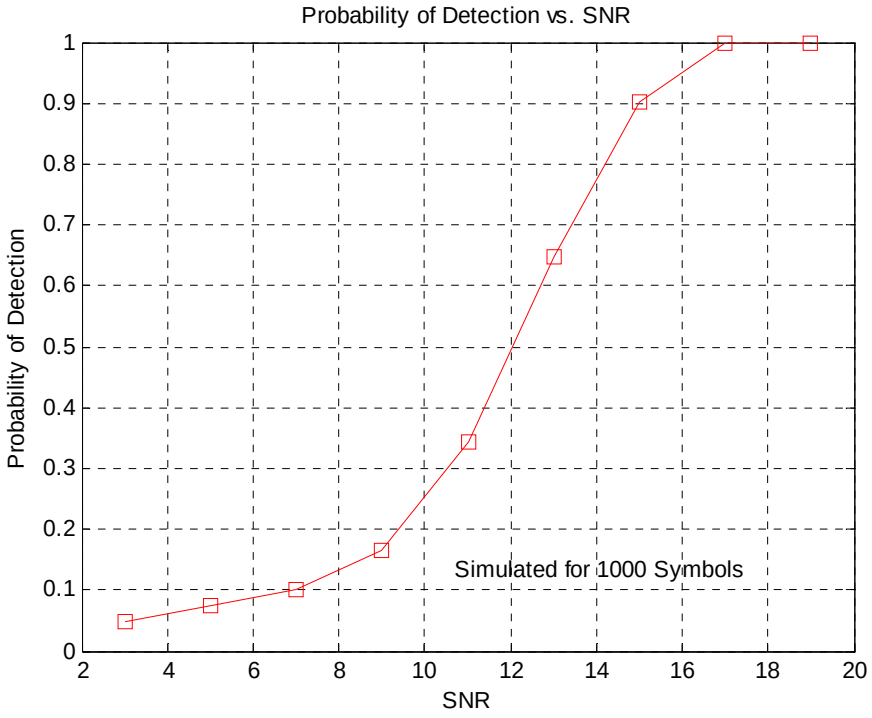

Figure 4.10: Probability of Detection vs. SNR for Case 1.

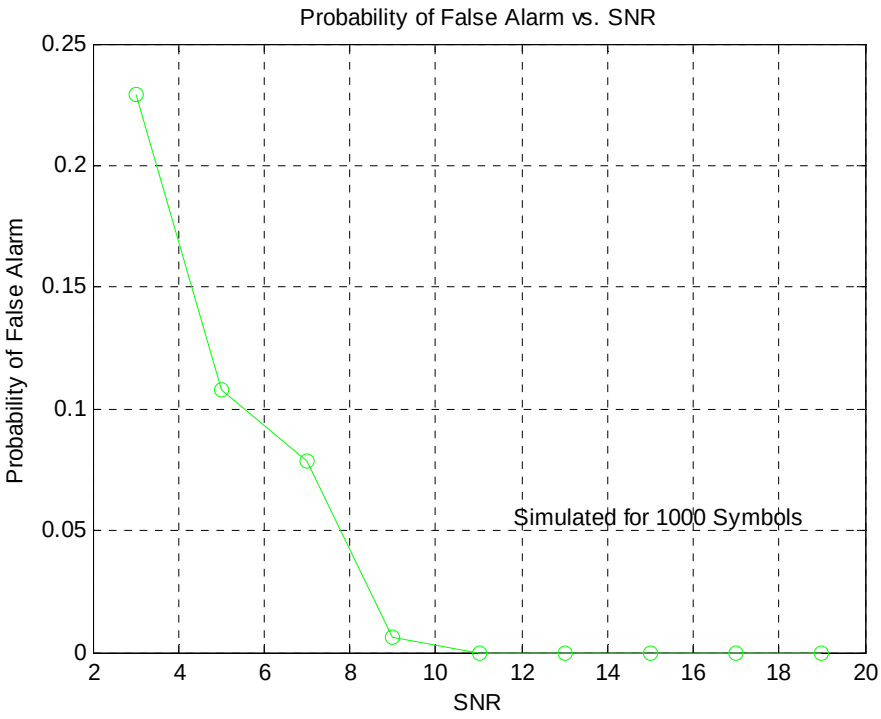

Figure 4.11: Probability of False Alarm vs. SNR for Case 1

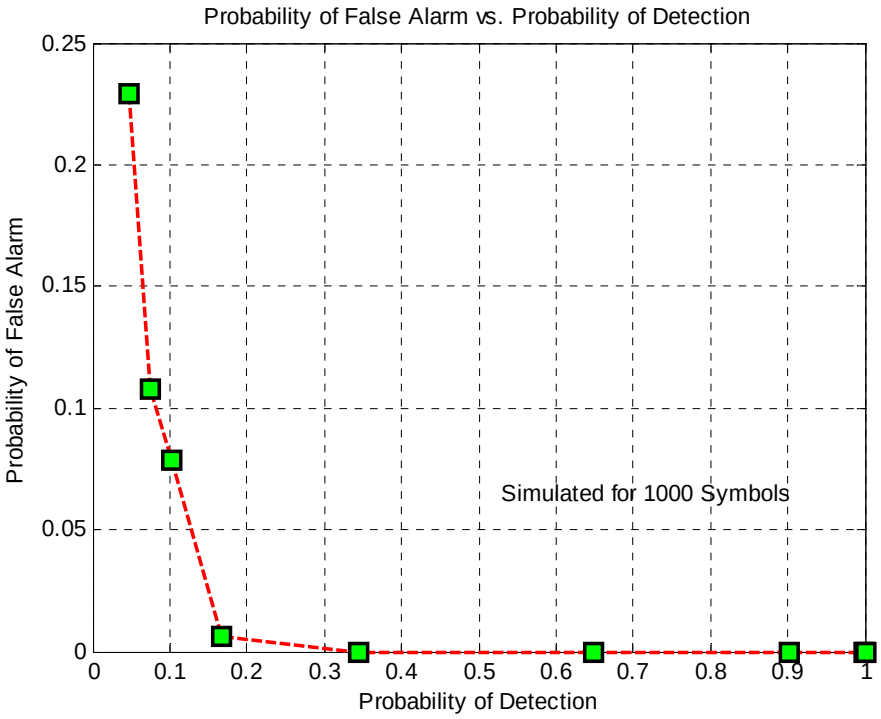

Figure 4.12: Probability of False Alarm vs. Probability of Detection for Case 1

The Probability of False Alarm is calculated only when the probability of detection is 1. From the above figures, we observe that the Probability of detecting a preamble increases with increasing SNR and the Probability of False Alarm for Synchronization decreases for increasing SNR. And at about 9dB, the probability of False Alarm is zero indicating that the correct integrator is selected for determining the synchronization instant.

4.6.2 Case 2 (NLOS 0-4m)

Case 2 deals with the non line of sight channel where the distance between the UWB nodes is less than 4m and having no direct line of sight. This is the case where the energy of the first cluster is not the strongest. This is typical of an NLOS channel where the first cluster penetrates through the obstacles and appears first at the receiver after severe attenuation from the obstacle that it passed through. The subsequent clusters which are reflected off the surfaces of the obstacles reach the receiver with a higher power.

Figure 4.13 shows the graph of Probability of Detection vs. SNR. Figure 4.14 shows the graph of Probability of False Alarm vs. SNR. The Probability of False Alarm is calculated only when the probability of detection is unity. Figure 4.15 shows the relation between Probability of Detection and the Probability of False Alarm for synchronization. And at about 7dB, the probability of False Alarm is zero indicating that the correct integrator is selected for determining the synchronization instant when the SNR is about 7dB. Also, it has to be noted that the Probability of Detection is unity only at 17dB. Even though the Probability of Detection is not unity from 7dB to 19dB, the Probability of False Alarm is equal to zero.

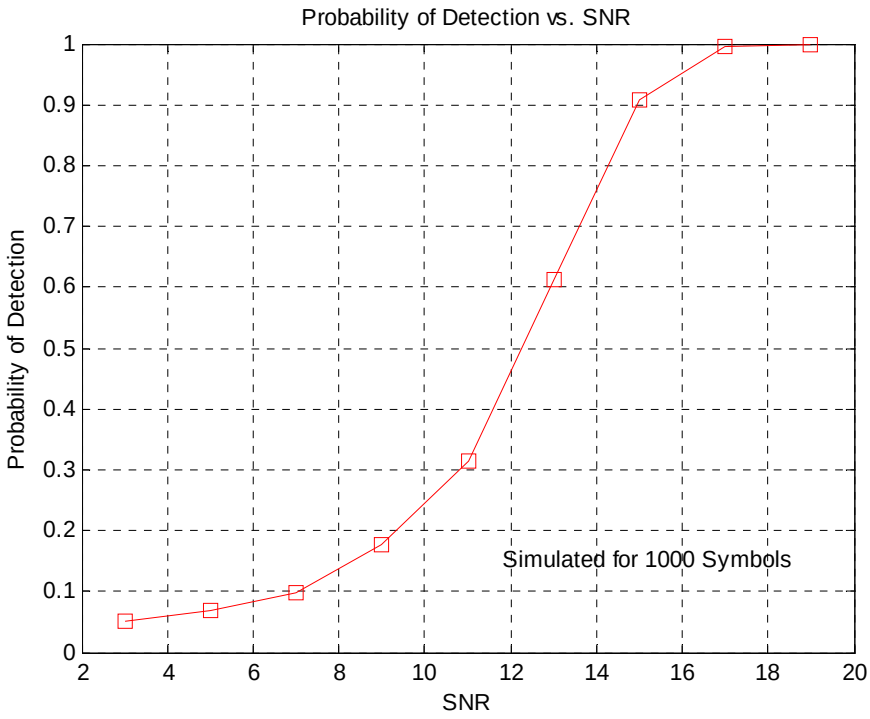

Figure 4.13: Probability of Detection vs. SNR for Case 2

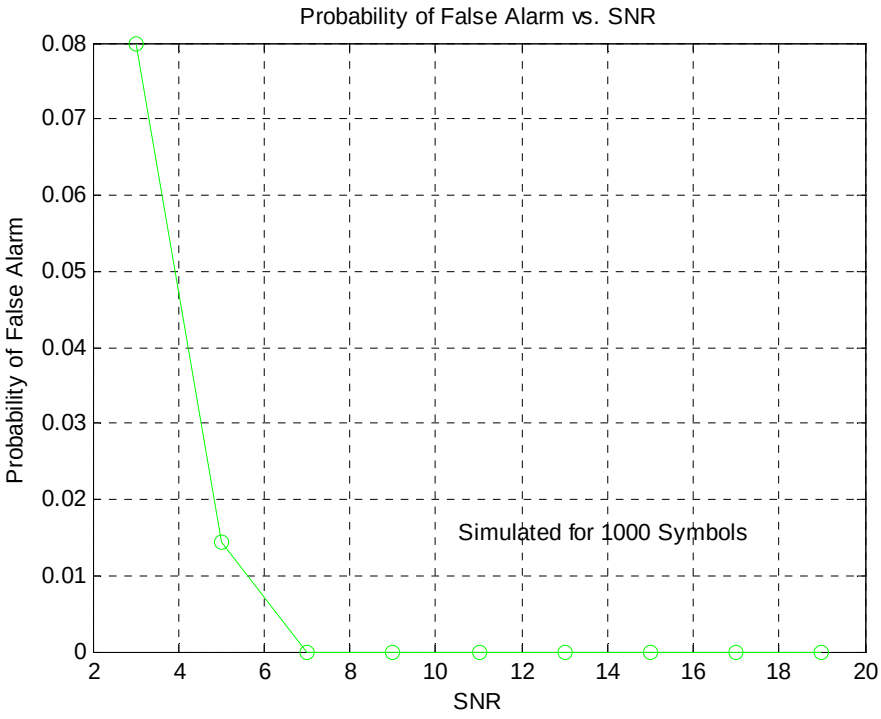

Figure 4.14: Probability of False Alarm vs. SNR for Case 2

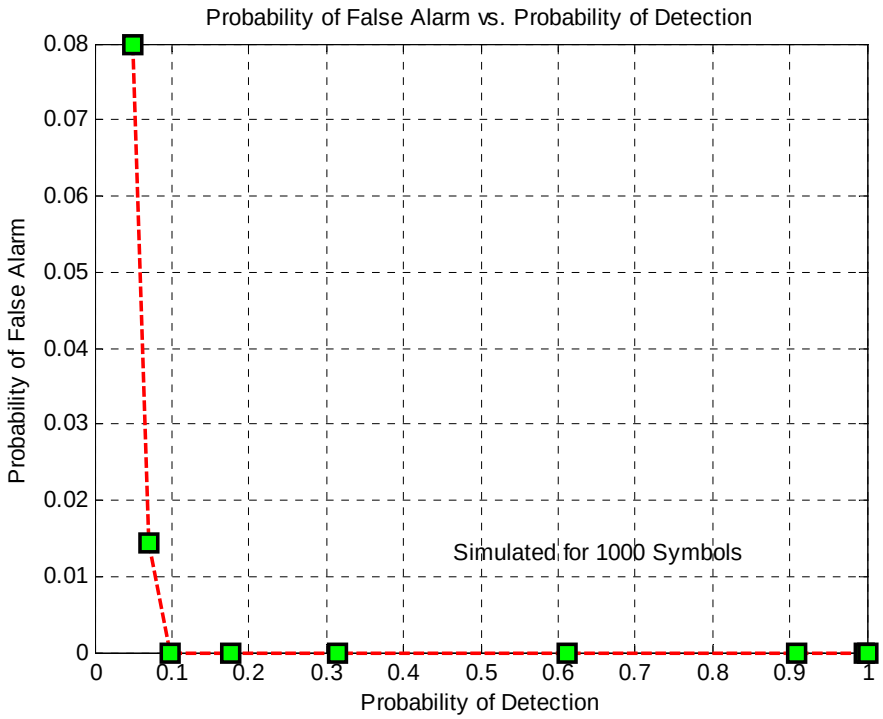

Figure 4.15: Probability of False Alarm vs. Probability of Detection for Case 2

4.6.3 Case 3 (NLOS 4-10m)

Case 3 deals with the non line of sight channel where the distance between the UWB nodes is between 4m and 10m. The pulses are received much longer in time than in cases 1 and 2. Also, the pulses are characterized by higher temporal dispersion of the energy than in cases 1 and 2. Figure 4.16 shows the graph of Probability of Detection vs. SNR. Figure 4.17 shows the graph of Probability of False Alarm vs. SNR and figure 4.18 shows the relation between Probability of Detection and the Probability of False Alarm for detection. At about 10dB, the probability of False Alarm converges to zero indicating that the correct integrator is selected for determining the synchronization instant when the SNR is about 11 dB.

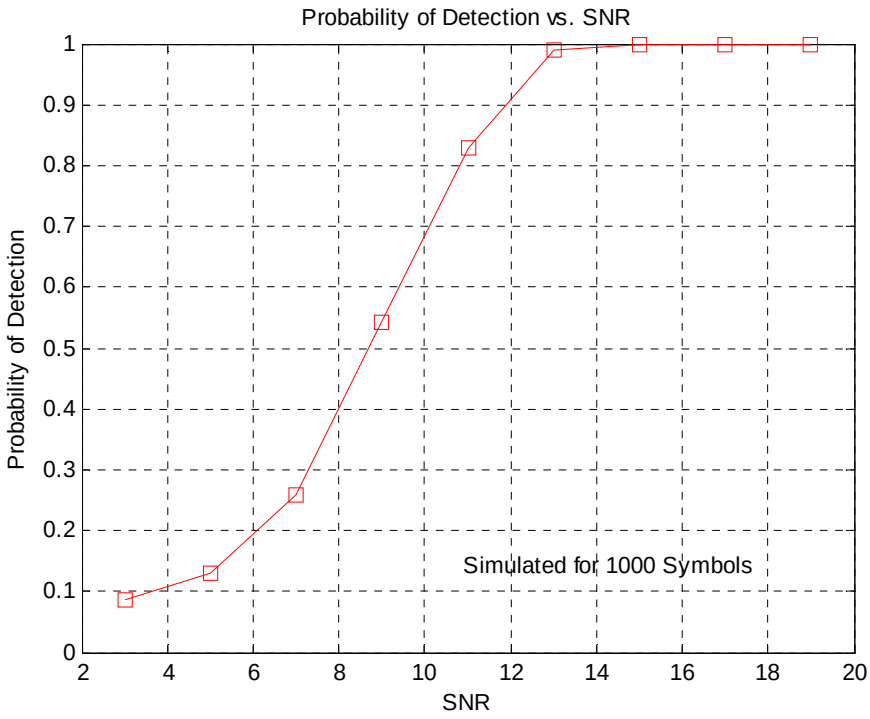

Figure 4.16: Probability of Detection vs. SNR for Case 3

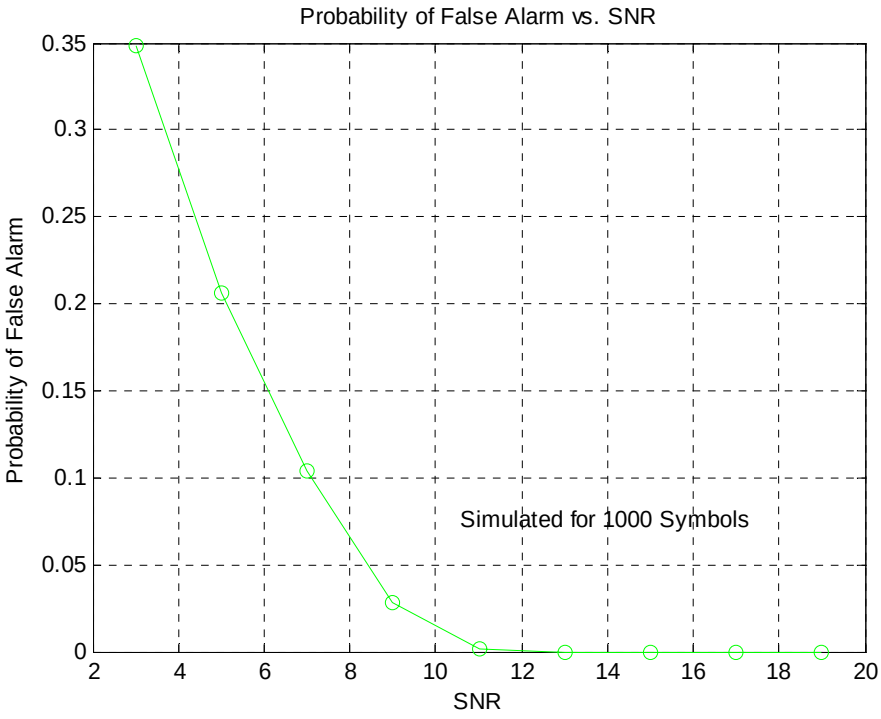

Figure 4.17: Probability of False Alarm vs. SNR for Case 3

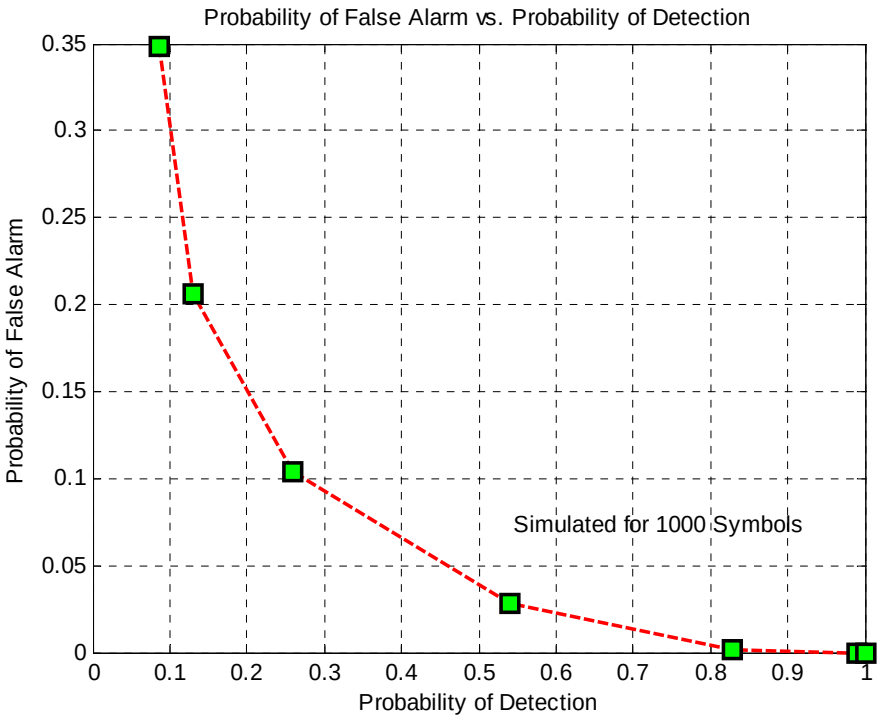

Figure 4.18: Probability of False Alarm vs. Probability of Detection for Case 3

4.6.4 Case 4 (Extreme NLOS)

Case 4 deals with the extreme non line of sight channel where the distance between the UWB nodes is between 4m and 10m. This is the channel which is most polluted with multipath energy as can be seen from the plot of the impulse response. Figure 4.19 shows the graph of Probability of Detection vs. SNR. Figure 4.20 shows the graph of Probability of False Alarm vs. SNR and figure 4.21 shows the relation between Probability of Detection and the Probability of False Alarm for detection.

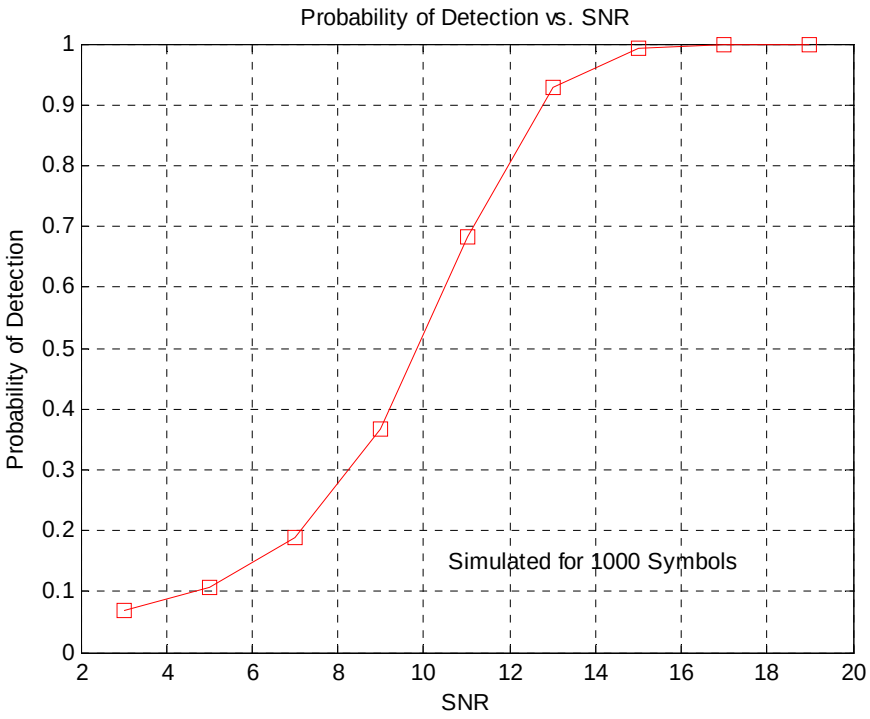

Figure 4.19: Probability of Detection vs. SNR for Case 4

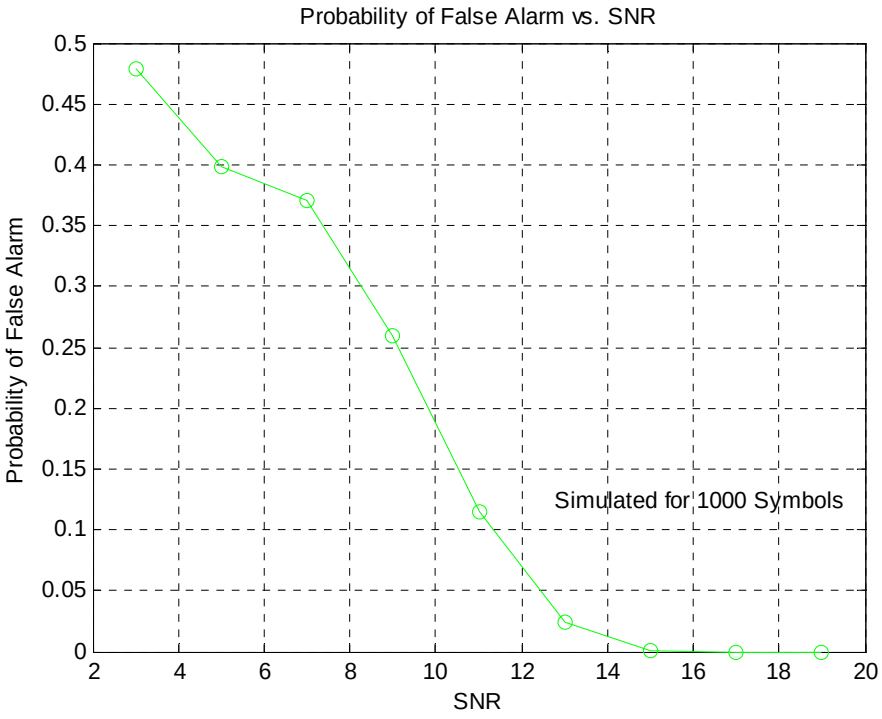

Figure 4.20: Probability of False Alarm vs. SNR for Case 4

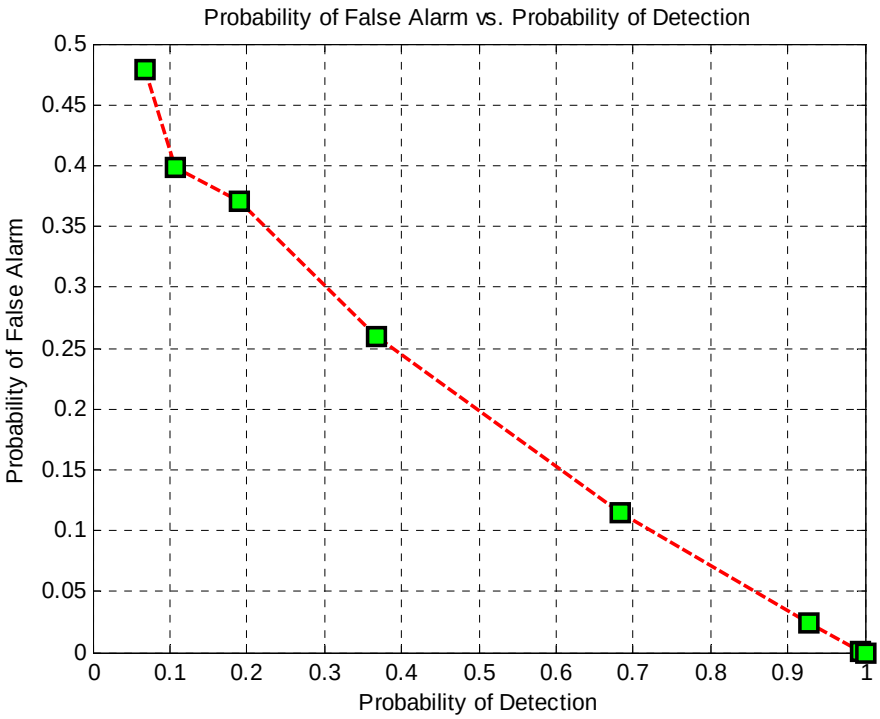

Figure 4.21: Probability of False Alarm vs. Probability of Detection for Case 4

4.7 Effect of Length of the Integrator on False Alarm

The length of the integrator is very important in the current energy collection approach of the synchronization. The length of the integrator has to be optimized in the energy collection approach to accommodate all the channel conditions. A short length of integration interval captures only a fraction of the desired signal energy and a long integration interval will capture the noise at the receiver. For example, from figure 3.5 of the impulse response for Case 4 (Extreme NLOS), the length of the integrator has to be at least 250ns to collect all the multipath energy.

4.7.1 Case 1 (LOS 0-4m)

For case 1, the length of the impulse response is approximately 80ns. Figure 4.22 shows the effect of integration window on the synchronization algorithm. The integration window is varied from 25ns to 100ns in 25ns intervals.

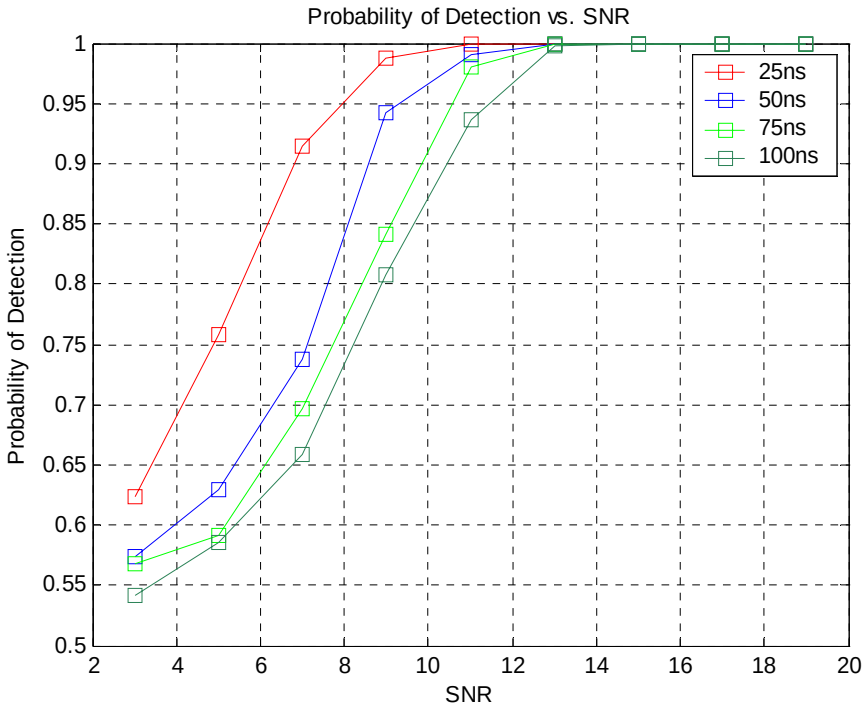

Figure 4.22: Probability of Detection vs. SNR for Case 1

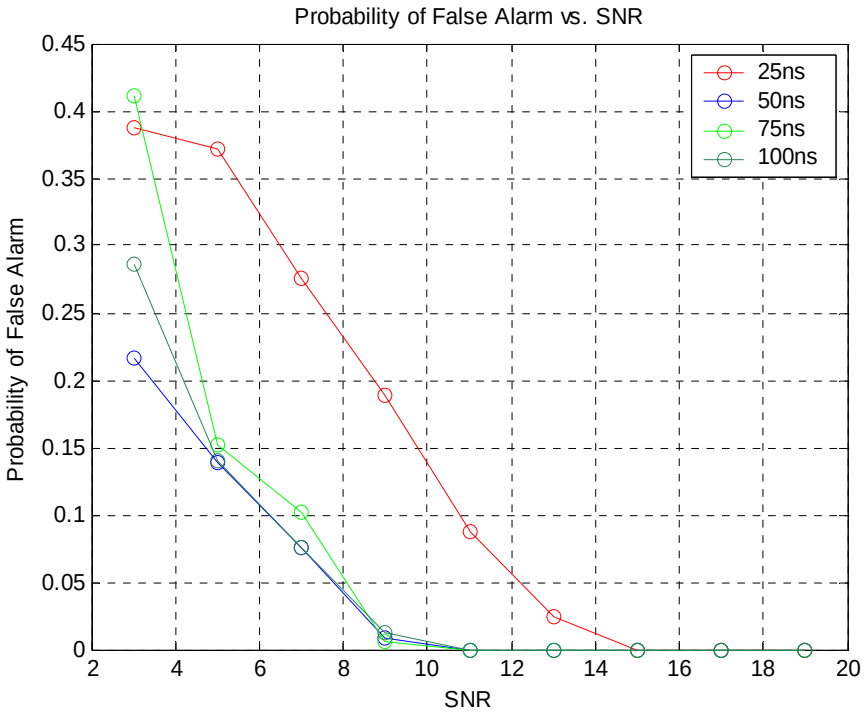

Figure 4.23: Probability of False Alarm vs. SNR for Case 1

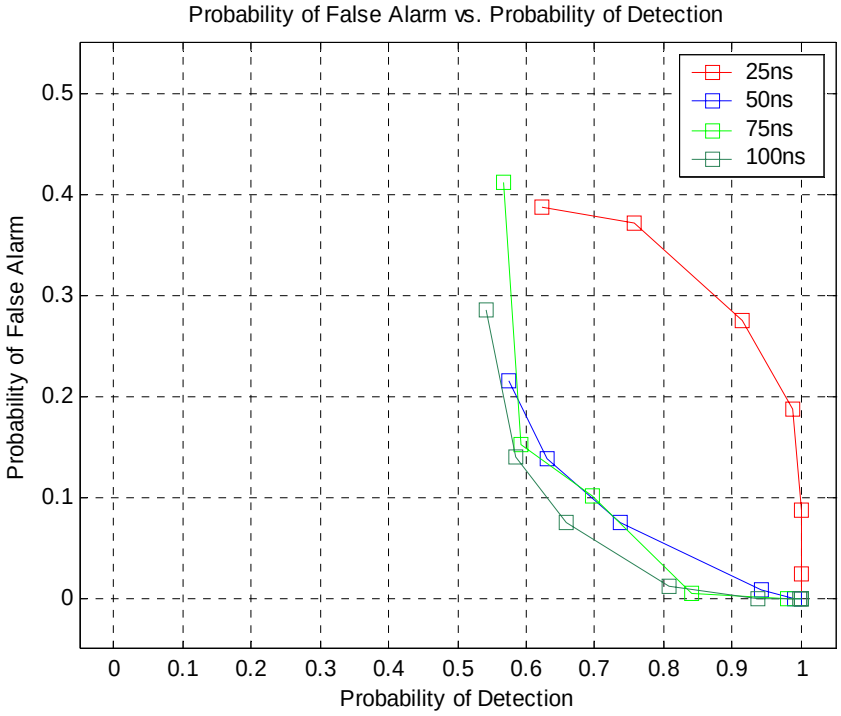

Figure 4.24: Probability of False Alarm vs. Probability of Detection for Case 1

From the above plots, we observe that when the length of the integrator falls below the impulse response time, the performance degrades drastically. When the integration window is greater than the effect of time dispersion of the transmitted energy, the Probability of False Alarm is almost the same. Having a higher integration window will capture the unwanted noise present at the receiver. Hence it is important to choose the optimum integration window without overkill. Any value above 50ns to 100ns gives the same performance approximately.

4.7.2 Case 2 (NLOS 0-4m)

For case 2, the length of the impulse response from Figure 3.3 shows that the energy of the pulses is extended from 0ns to little above 75ns. Figure 4.25, 4.26 and 4.27 shows the performance of the algorithm at various integrator windows of 50ns, 75ns, 100ns and 125ns.

From the plots, we can observe that the performance of the algorithm gets better as the length of the integrator is increased. The minimum length of the integrator should be greater than the impulse response time of about 80ns for case 2. The length of the integrator can be varied according to the channel conditions for optimal performance of the algorithm.

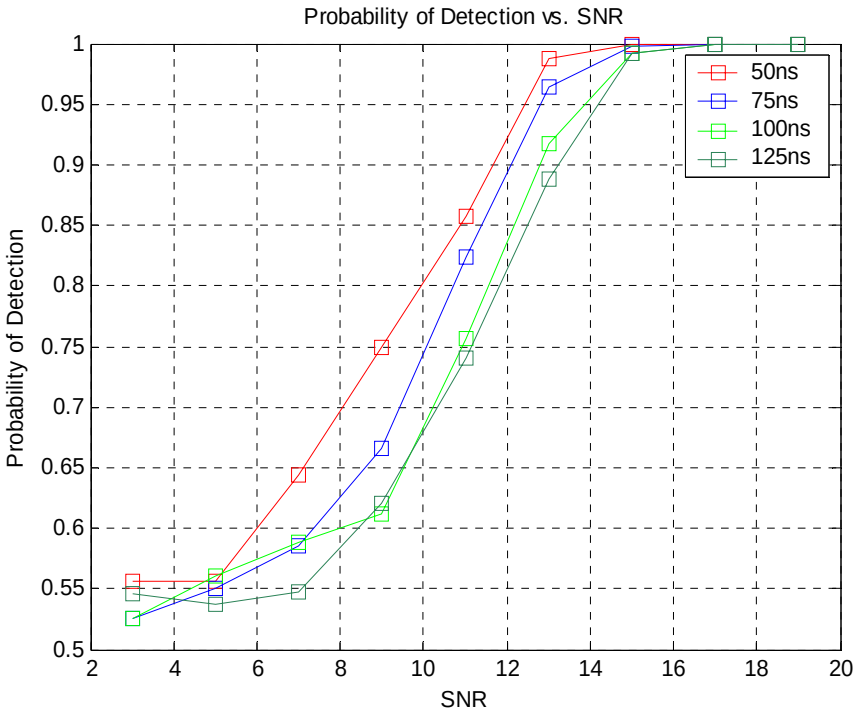

Figure 4.25: Probability of Detection vs. SNR for Case 2

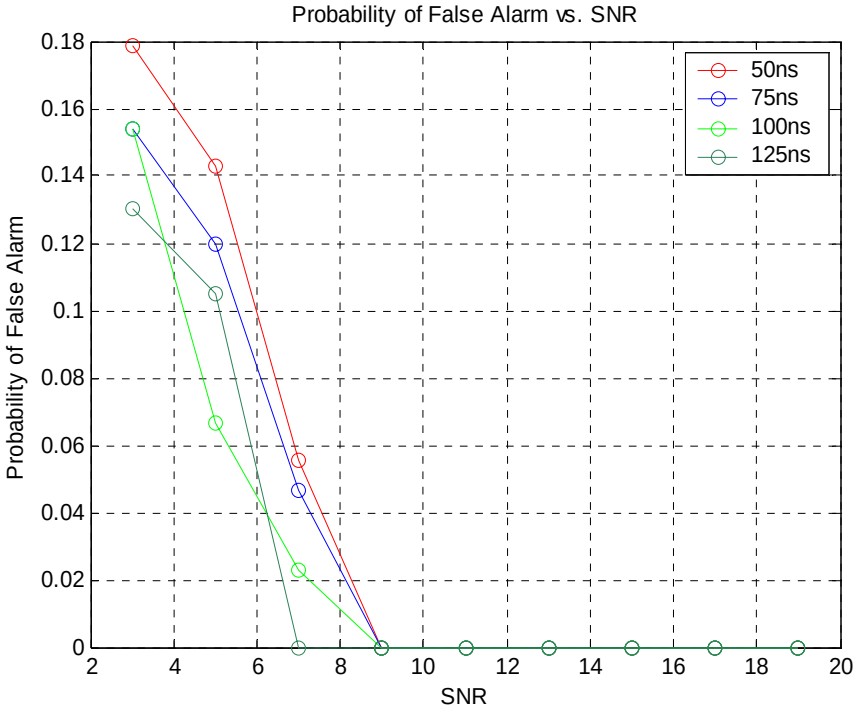

Figure 4.26: Probability of False Alarm vs. SNR for Case 2

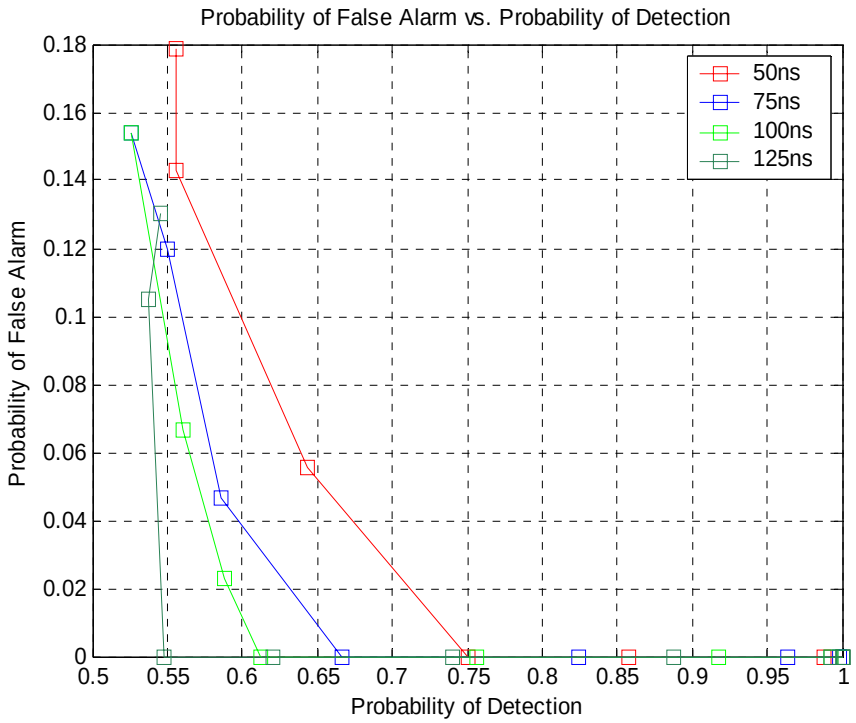

Figure 4.27: Probability of False Alarm vs. Probability of Detection for Case 2

4.7.3 Case 3 (NLOS 4-10m)

Case 3 deals with the Non Line of Sight channel model with impulse response time of about 150ns as shown in figure 3.4. Figures 4.28, 4.29 and 4.30 show the plots for various integration windows ranging from 75 to 150ns in 25ns interval.

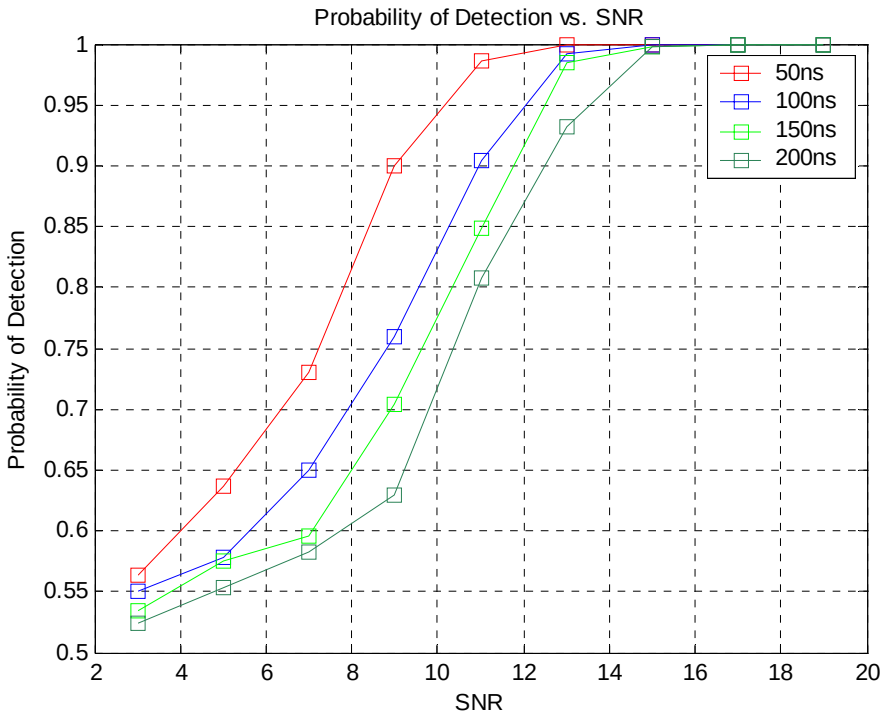

Figure 4.28: Probability of Detection vs. SNR for Case 3

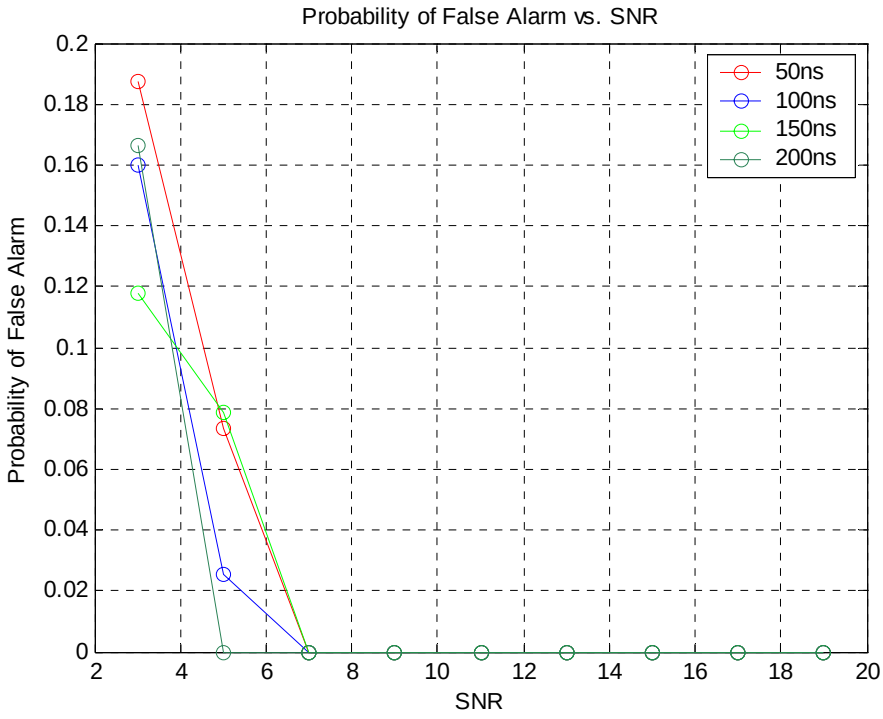

Figure 4.29: Probability of False Alarm vs. Probability of Detection for Case 3

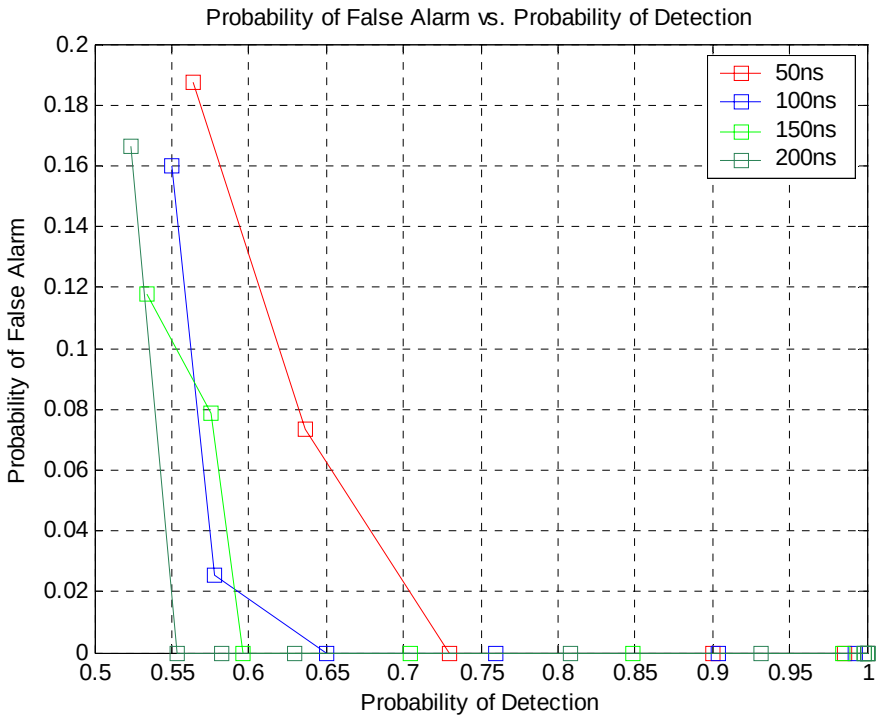

Figure 4.30: Probability of False Alarm vs. Probability of Detection for Case 3

From the above plots, we observe that the performance of the algorithm gets better as the length of the integrator approaches the channel impulse response time for Non Line of Sight channels.

4.7.4 Case 4 (Extreme NLOS)

Case 4 deals with the extreme Non Line of Sight channel conditions. From figure 3.5, we observe that the impulse response is about 250ns. Figures 4.31, 4.32 and 4.33 show the performance of the algorithm when the integration window is varied from 225ns to 300ns.

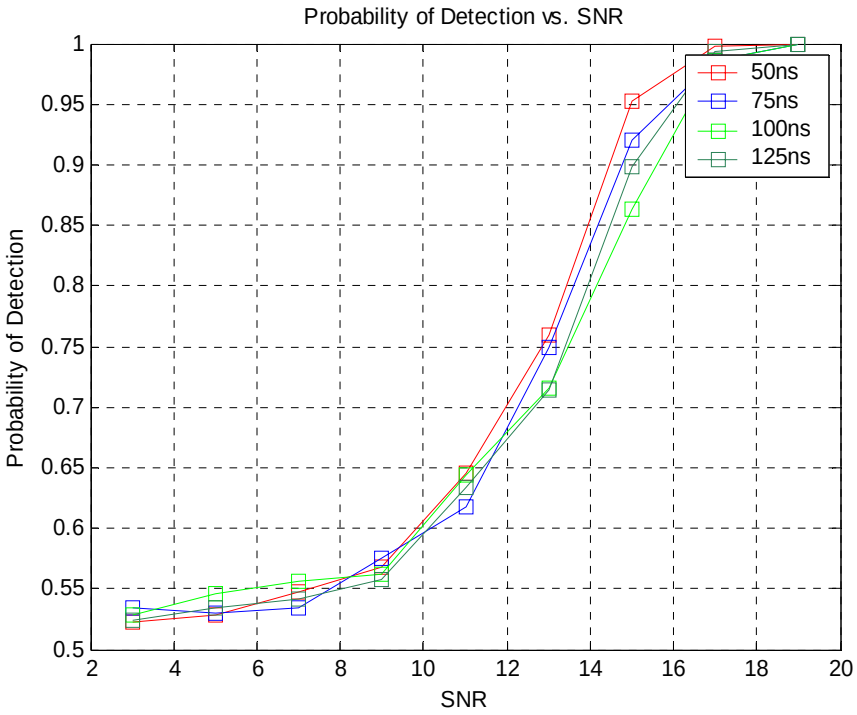

Figure 4.31: Probability of Detection vs. SNR for Case 4

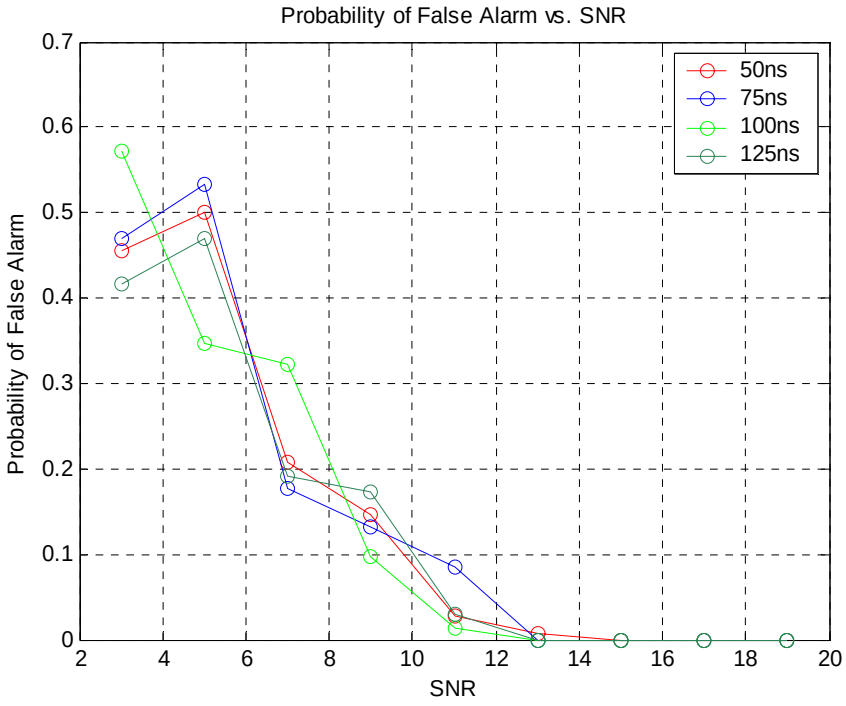

Figure 4.32: Probability of False Alarm vs. SNR for Case 4

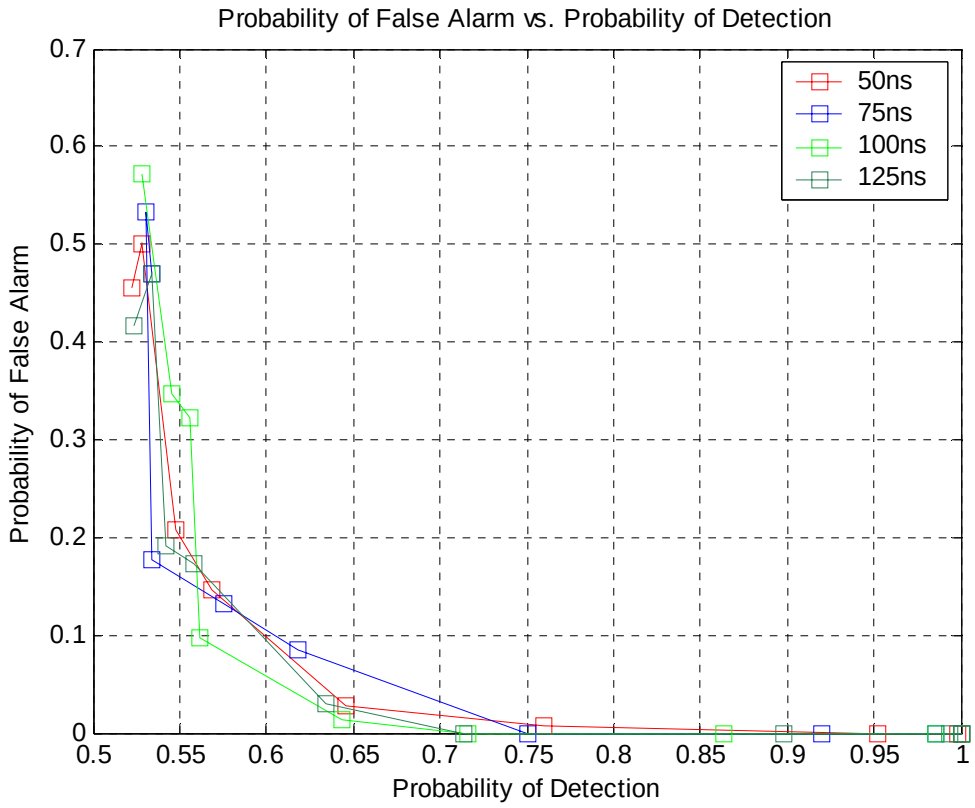

Figure 4.33: Probability of False Alarm vs. Probability of Detection for Case 4

From the plots, we observe that the performance of the algorithm is almost the same irrespective of the length of the integrator for Extreme NLOS case. From the impulse response graph, considerable concentration of received energy is observed for a significant period of time for a single pulse. As discussed earlier, each preamble bit is specified by 8 closely spaced pulses producing several multipath components that span multiple integrators resulting in a higher False Alarm rate. As the multipath energy is spread for a long period and because of its random nature, the performance of the algorithm remains the same for integrator lengths varying from 50ns to 125ns.

4.8 Conclusion

Probability of False Alarm for Synchronization has been chosen to analyze the performance of the algorithm under various channel conditions of the modified Saleh Valenzuela channel model. Figure 4.34 shows that the Probability of Detection increases with increasing SNR, and, from figure 4.35, we observe that the Probability of False Alarm decreases with increasing SNR as expected. The Probability of False Alarm is significantly high for extreme NLOS case (case 4), and the energy collection is better suited for the remaining channel models for a given SNR. This is expected because the multi path energy is spilled all over the time period in case 4 and hence the energy collection receivers may not perform better for synchronization in extreme NLOS cases.

The algorithm has to be optimized for each channel condition by taking the channel impulse response into account. It has been shown that as long as the length of the integrators is greater than the effect of time dispersion of the energy, the algorithm performs better. Also, the combination of the number of preamble bits and data bits according to channel conditions gives optimum results.

Figure 4.34, 4.35 and 4.36 show the combined plots for Probability of Detection and False Alarm for all channel conditions discussed and gives the comprehensive idea of the performance of the energy collection based synchronization. The length of the integrator is chosen to be 250ns. It is to be noted that the probability of false alarm for synchronization is calculated only when there is a detection of the preamble sequence.

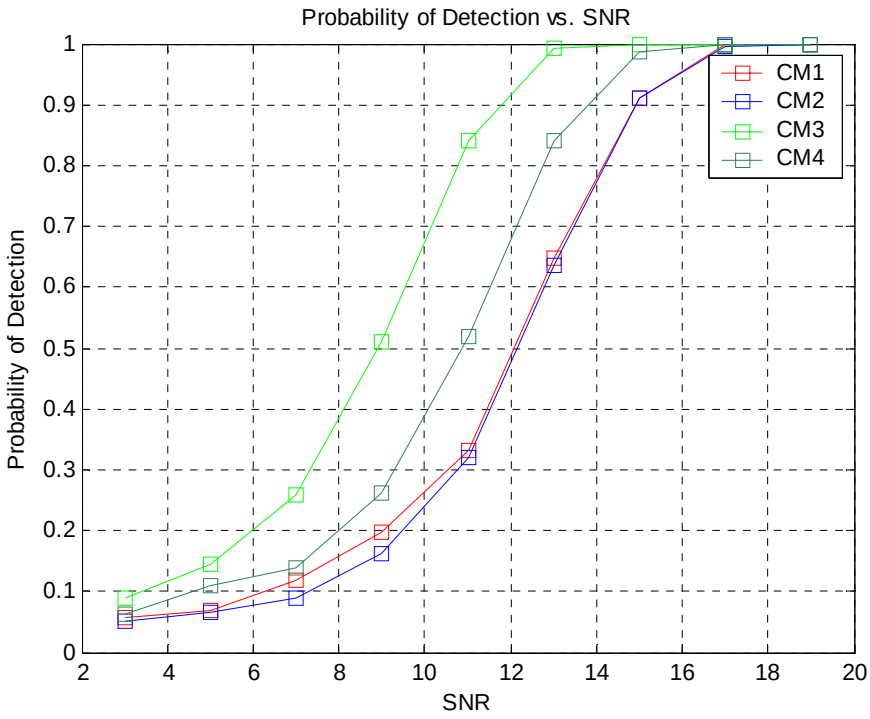

Figure 4.34: Probability of Detection vs. SNR for all Cases

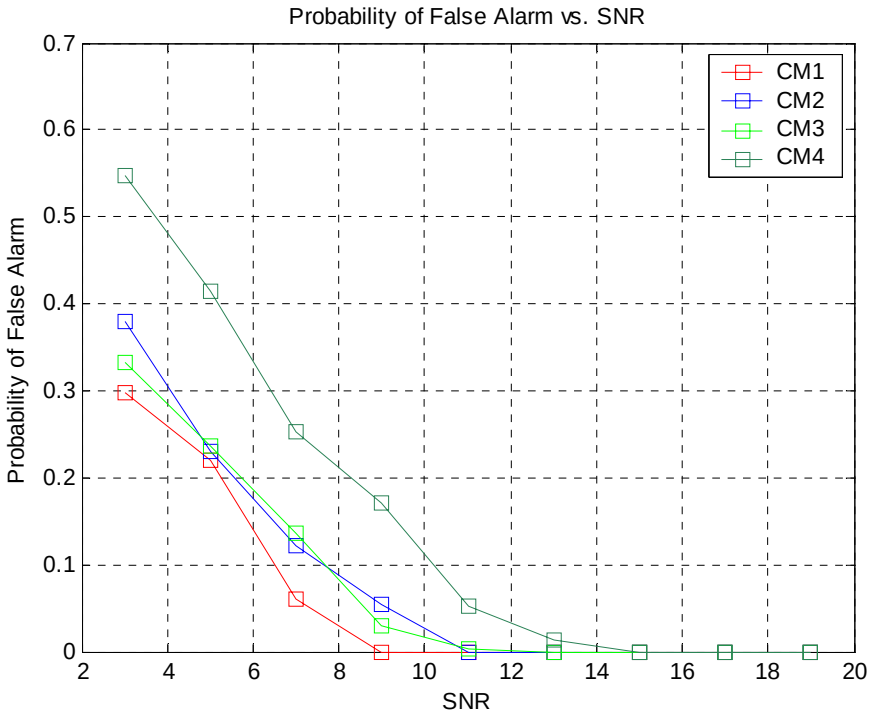

Figure 4.35: Probability of False Alarm vs. SNR for all Cases

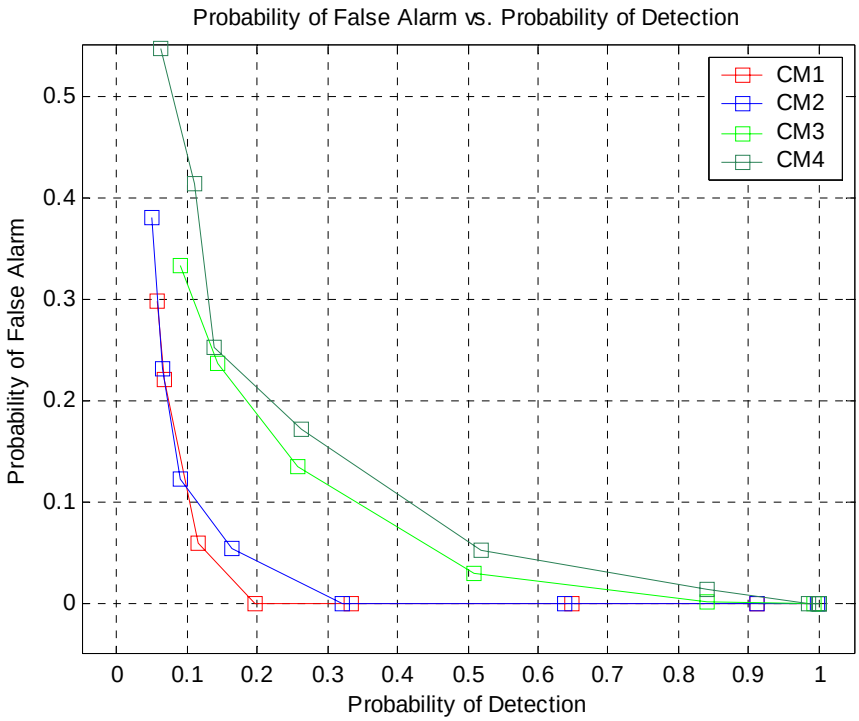

Figure 4.36: Probability of False Alarm vs. Probability of Detection

From the figures, we conclude that the false alarm rate is higher for Extreme NLOS channel conditions (case 4). For the remaining cases, false alarm rate remains approximately similar and improves as the length of the integrator approaches the impulse response time. Also, from figure 4.36, we observe that the probability of false alarm approaches unity as the probability of detection is greater than 0.6 for cases 1 and 2. For case 3 and 4, PFA (Probability of False Alarm) approaches zero for a greater Pd (Probability of Detection).

Chapter 5

Conclusions and Future Work

Synchronization is very important in pulse based UWB systems. Synchronization errors lead to bit errors at low SNR values and hence adversely affects the data rate of the overall UWB system as well as dissipate more power because of retransmissions. The thesis evaluated the performance of energy collection receivers for synchronization of impulse based Ultra Wide Band systems. A comprehensive and graphical description of simulation was presented. The performance of the algorithm under various channel conditions was studied. From the simulations, we can conclude that the algorithm performs well for cases 1, 2 and 3, and, the Probability of False Alarm for synchronization is comparably the same. The performance degrades for Extreme NLOS case because of the nature of the channel polluted heavily with multipath energy.

The complexity of the algorithm can be changed as needed for various channel conditions. The precision of the algorithm can be increased by increasing the number of integrators and/or by increasing the spacing between the integrators. Best values are to be chosen without overkill as large number of integrators dissipates more energy due to excessive computation.

The effect of the size of the integrator window on the performance of synchronization algorithm using energy collection receivers is studied for various channel conditions. It is

concluded that the integrator window should be at least the amount of time dispersion of the transmitted energy for best performance.

There are still a lot of open questions that should be addressed in future research. Some items where more research can be done include studying the performance of the algorithm with various pulse shapes, like the Gaussian modulated sinusoidal pulses and evaluating the performance of the algorithm when multiple users are present. Implementation of Rake receivers and MIMO techniques is also a significant research topic by itself. Future research can focus on using Frequency Hopping UWB synchronization when multiple users are present in a network.

Using these innovative techniques involves increasing the complexity of the circuitry but as with any communications system, the systems engineer will have to make a trade off between complexity and performance. The right combination of these in implementing UWB synchronization techniques depends on the specific applications. Reaping the benefits of huge bandwidth associated with Ultra Wideband systems while keeping the receiver architecture reasonably simplistic is the ultimate design goal for the hardware.

References

[1] FCC, "Revision of Part 15 of the Commission's Rules Regarding Ultra-Wideband Transmission Systems", First Report and Order, ET Docket 98-153, FCC 02-8, adopted/released Feb. 14/Apr 22, 2002.

[2] http://www.instat.com/newmk.asp?ID=1679

[3] http://www.wimedia.org/

[4] http://www.uwbforum.org

[5] http://www.cs.wustl.edu/~jain/cse574-06/ftp/phy_trends/index.html#sec2.1.2

[6] Rabbachin, A.; Opperman, I.; "Synchronization Analysis for UWB systems with a Low-Complexity Energy Collection Receiver", International workshop on Ultra Wideband Systems, 2004, Joint with Conference on Ultra Wideband Systems and Technologies.

[7] F. Ramirez-Mireles and R. A. Scholtz, "System performance analysis of impulse radio modulation", in *Proc. Radio and Wireless Conference,* Colorado Springs, CO, USA, Aug. 1998, pp.67-70.

[8] K. Pourvoyeur, A. Stelzer, G. Oβberger, T. Buchegger, and M. Pichler, "Wavelet-based Impulse Reconstruction in UWB-Radar", in *Proc. IEEE MTT-S International Microwave Symposium (IMS 2003).*

[9] Dongsong Zeng, Annamalai A. Jr., Zaghloul, A. I; "Pulse Shaping Filter Design in UWB System", *IEEE Conference on Ultra Wideband Systems and Technologies, 2003.*

[10] http://www.eng.usf.edu/~iguvenc/EEL4512/Project/Matlab_Project.m

[11] M. Di Benedetto, G. Giancola, "*Understanding Ultra Wide Band Radio Fundamentals*", Prentice Hall, 2000.

[12] Q. H. Spencer, B. D. Jeffs, M. A. Jense, A. L. Swindlehurst, "Modeling the Statistical Time and Angle of Arrival Characteristics of an Indoor Multipath Channel," IEEE JSAC, Vol. 18, No. 3, March 2000.